Mechanisms Governing the Persistence and Diurnal Cycle of a Heavy Rainfall Corridor

STANLEY B. TRIER, CHRISTOPHER A. DAVIS, AND RICHARD E. CARBONE

National Center for Atmospheric Research, Boulder, Colorado*

(Manuscript received 8 May 2014, in final form 7 July 2014)

ABSTRACT

Observations and convection-permitting simulations are used to study a 12-day warm-season heavy precipitation corridor over the central U.S. plains and Mississippi River valley regions. Such precipitation corridors, defined by narrow latitudinal widths (~3°–4°) and only modest north–south drifts of their centroids (<2° day^{-1}), often yield extreme total precipitation (100–250 mm), resulting in both short-term and seasonal impacts on the regional hydrologic cycle.

The corridor precipitation is predominately nocturnal and located several hundred kilometers north of a quasi-stationary surface front. There, hot, dry air from the daytime boundary layer located underneath a persistent upper-level anticyclone requires large vertical displacements along the axis of the southerly low-level jet (LLJ) above the front to eliminate convection inhibition (CIN). Composites reveal ~500 J kg^{-1} of average convective available potential energy (CAPE) when this air reaches the southern edge of the precipitation corridor. Despite the relatively modest CAPE, convection is favored by the large reductions in CIN along the vertical displacements and by high ambient midtropospheric relative humidity located above, which is influenced by persistent nightly convection in the region.

Though internal feedbacks resulting from the large nightly spatial coherence of convection (including enhanced midtropospheric relative humidities and frontogenetic daytime sensible heat flux gradients owing to residual cloudiness) are favorable for maintaining the corridor, its persistence is most sensitive to large-scale external factors. Here, changes to the intensity and position of the large-synoptic upper-tropospheric anticyclone are associated with changes in the frequency of strong LLJs and the surface frontal position, dramatically affecting the intensity and stationarity of the precipitation corridor.

1. Introduction

Among the aspects that distinguish deep convection in the lee of major midlatitude (Carbone et al. 2002; Wang et al. 2004) and subtropical (e.g., Rasmussen and Houze 2011) mountain ranges from most convection elsewhere are its propensity to propagate eastward and its most frequent occurrence at night. In the central United States, the well-known nocturnal maximum of warm-season precipitation (Wallace 1975) results primarily from organized mesoscale convective systems (MCSs) and complexes (MCCs; Maddox, 1980, 1983).

The tendency for MCSs and MCCs to occur in succession over approximately the same location was recognized by Fritsch et al. (1986), who noted the hydrologic importance of these serial convective events over the central U.S. agricultural region. Tuttle and Davis (2006, hereinafter TD06) discussed how multiday convective episodes are often confined to narrow (~3°–4°) latitudinal "corridors." In their 5-yr central U.S. climatology, TD06 found that most heavy precipitation corridors last 1–2 days, although extreme events lasting > 4–5 days (e.g., Wetzel et al. 1983) are not rare, having recurrence frequencies of ~1 yr^{-1}. Together, these long-lived and more common shorter-lived corridors constitute a significant fraction of the central U.S. warm-season precipitation. In the current paper we use observations and sensitivity studies with a convection-permitting model to determine factors influencing the persistence and diurnal cycle of a particularly long-lived heavy precipitation corridor (20–31 July 1998).

The longest-lived corridors in TD06 were associated with repeatable external atmospheric forcings. These

* The National Center for Atmospheric Research is sponsored by the National Science Foundation.

Corresponding author address: Stanley B. Trier, National Center for Atmospheric Research, P.O. Box 3000, Boulder, CO 80307-3000.
E-mail: trier@ucar.edu

DOI: 10.1175/JAS-D-14-0134.1

included strong 900-hPa geopotential height anomalies, which signify the presence of lower-tropospheric fronts. Such fronts are distinct from those that accompany baroclinic cyclones. The strong, but shallow fronts of interest in the current study typically occur in mid- to late summer and are often quasi-stationary (e.g., Kane et al. 1987). The origin of such fronts is not always clear and could be influenced by a variety of factors including lower-tropospheric flow deformation and the cumulative effects of antecedent convection. These fronts also have similarities to East Asian mei-yu fronts, where multiday quasi-stationary precipitation episodes have also been simulated and analyzed (Sun and Zhang 2012; Wang et al. 2012).

Maddox (1983) noted that the southerly nocturnal low-level jet (LLJ, e.g., Stensrud 1996) is an important general feature of MCC environments since they are often associated with warm advection and vertical motions near their northern terminus. TD06 noted that the long-lived corridors had the strongest 900-hPa meridional jets. LLJ anomalies have been noted in studies of individual seasonal precipitation anomalies, including the central U.S. floods of 1993 (Arritt et al. 1997) and extreme hydroclimatic episodes in general (e.g., Weaver and Nigam 2011).

While strong lower-tropospheric gradients are evident in long-lived corridor environments, middle- to upper-tropospheric features are often relatively benign. TD06 found a large-scale upper-tropospheric anticyclone to be present up to the southern edge of the corridor in composite conditions for long-lived corridors. North of the precipitation corridor the upper-level flow contained much stronger westerlies, but had limited, if any, convective available potential energy (CAPE). Therefore, environments that support corridors are often conducive to dry conditions in juxtaposed locations, making corridors hydrologically significant beyond their relatively narrow latitudinal confines.

The Maddox (1983) composites reveal that weak deep tropospheric disturbances, often referred to as short waves, frequently occur in MCC environments. However, recent studies (e.g., Trier et al. 2010; Sun and Zhang 2012) have simulated idealized corridors using temporally periodic lateral boundary conditions that mitigate the effects of such transient disturbances that are not induced internally by factors such as deep convection or terrain. Nevertheless, while Tuttle and Davis (2013) noted that short waves did not influence climatological observed local diurnal cycles of warm-season convection, they emphasized that their influence on individual cases could be substantial depending on their phasing with the local diurnal cycle. Thus, their influence on actual cases of long-lived precipitation corridors remains an open question.

In addition to the aforementioned external meteorological factors, internal feedbacks related to heavy precipitation could potentially influence especially long-lived corridors. In particular, the nightly occurrence of widespread deep convection in approximately the same location influences lower-tropospheric baroclinity through the cooling effects of downdrafts associated with precipitation. Such baroclinity can be enhanced further by daytime differential heating owing to residual cloudiness near regions experiencing widespread and long-lived nocturnal convection. Finally, increases of soil moisture within the corridor are likely to affect the partition between sensible and latent heat fluxes. In this vein, Findell and Eltahir (2003a,b) argued that soil moisture can influence the triggering of new convection. Thus, a fully three-dimensional convection-allowing model, coupled to a land surface model, is employed in the current study to examine possible roles of different external and internal forcings in the persistence of a particularly long-lived regional precipitation event.

2. Observations of the July 1998 heavy precipitation corridor

The heavy precipitation corridor we examine was illustrated briefly in TD06 as an example of an extreme corridor lasting 12 days. It commenced on 19 July 1998 and was centered near 42°N until 22 July, by which time it became displaced southward and was located between 37° and 40°N for the remainder of its duration. In the current study we focus on the latter 9 days of the event (23–31 July) during which the corridor was most stationary.

The latitudinal confinement of the corridor during this 9-day period is evident in a map of the total nocturnal (2000–0800 LST) rainfall accumulation (Fig. 1a) from Stage-4 analyses, which combine radar and rain gauge measurements (Fulton et al. 1998). The maximum rainfall band exceeding 100 mm (Fig. 1a) is situated on the north side of a strong northwest–southeast-oriented lower-tropospheric baroclinic zone revealed by a composite 0000 UTC (1800 LST) Eta Model surface analysis (Fig. 1b) representing conditions near the onset of nightly convection during the 9-day period. Note that the CAPE of the most unstable air parcel in a vertical column (MUCAPE) is enhanced within the western part of the baroclinic zone where the corridor convection first originates, while it is suppressed at the same longitudes (~−102° to −94°) outside of the baroclinic zone, particularly beyond its southwestern edge (Fig. 1b). The enhancement of MUCAPE within or very close to the location of the surface baroclinic zone is a common feature of corridors evident in the TD06 climatology.

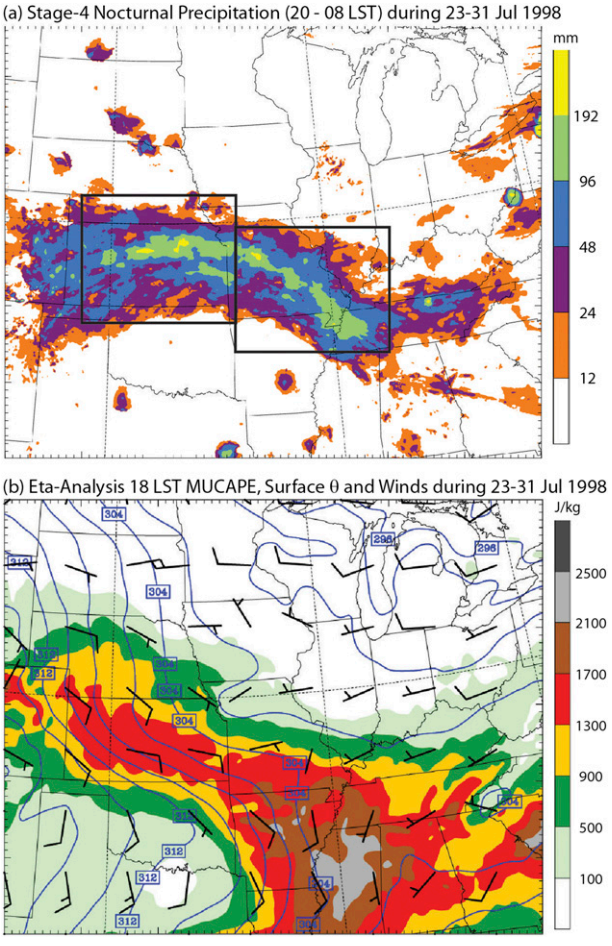

FIG. 1. (a) 9-day total nocturnal (0200–1400 UTC) precipitation from Stage-4 analyses of 23–31 Jul 1998. (b) Corresponding 9-day-averaged Eta Model analysis of the CAPE of the most unstable (highest θ_e) 50-hPa-averaged air parcel in a vertical column (MUCAPE), surface winds, and surface potential temperature at 0000 UTC.

Rainfall events of varying intensity occurred each night (Fig. 2a) over the central plains part of the corridor indicated by the westernmost box in Fig. 1a. A Hovmöller diagram (Fig. 2b) prepared using the Stage-4 hourly rainfall analyses averaged within the latitudinal confines of the corridor shows daily afternoon initiation near the lee of the Rockies (~−105°) and subsequent eastward progression of rain overnight beyond the central plains (95°W) for a majority of events. These are common aspects of the diurnal cycle of rainfall in the central United States during active warm-season periods (Carbone et al. 2002).

Closer inspection of Fig. 2b indicates decreases in the downward slope of rain streaks overnight in central plains longitudes for several of the most prominent cases, implying increases in phase speed. However, animations of radar reflectivity data (not shown) revealed that the long-lived rain streaks in Fig. 2b rarely comprised individual MCSs that propagated continuously across the entire longitudinal extent of the central plains.

An example from the spatiotemporal section of the Hovmöller diagram outlined by the dotted red rectangle in Fig. 2b shows contrasting modes of mesoscale convective organization overnight on the plains (Fig. 3). As the precipitation reached −100° (Figs. 2b and 3a), the primary feature was an eastward-propagating asymmetric squall-type MCS (e.g., Houze et al. 1990; Brandes 1990; Scott and Rutledge 1995). While this feature weakened overnight, locally forced convection (aligned parallel to the surface front) developed successively eastward (Figs. 3b,c). The organization in this next wave of convection is more akin to the training line-adjoining stratiform (TL/AS) archetype described by Schumacher and Johnson (2005). Areas influenced by MCSs of this type are particularly prone to flash flooding since convective cells can redevelop upstream and subsequently traverse previously affected locations.

In the current example local rainfalls of up to 4 in. (~100 mm), resulting in flooding, were reported in Kansas City, Missouri, during the near-sunrise hours (NCDC 1998). According to TD06, locally forced convective precipitation is most common in corridors with stronger than average southerly nocturnal LLJs, which would in turn promote stronger mesoscale lifting in frontal environments such as that of the current case (section 5).

Time–latitude Hovmöller diagrams, averaged for 600 km from ~−101.5° to −94° longitude (Fig. 4), convey the spatiotemporal variations in the environment influencing the location and intensity of the rainfall corridor. This longitudinal swath is in a similar location but is slightly larger than that used by TD06 in their heavy rainfall corridor climatology. Our averaging region (Fig. 2b, thick vertical lines) intersects the most intense portion of the time-averaged lower-tropospheric front (cf. Fig. 1b) and contains the western (onset) locations of nocturnal rains (Fig. 1a).

The nightly rainfall events in the corridor occur within the latitude band of the strongest zonal component of lower-tropospheric vertical shear (Fig. 4a), which is supportive of eastward-propagating MCSs through horizontal vorticity balance mechanisms (e.g., Rotunno et al. 1988). However, the vertical shear is also indicative, from thermal wind considerations, of a strong lower-tropospheric front, which appears most germane to the organization of the corridor precipitation. In particular, the rainfall centers are located within or near the 850-hPa potential temperature θ gradient (Fig. 4b). The rainfall centers also correspond well to the 850-hPa meridional wind maxima, both in their locations near the jet terminus, and in their timing (Fig. 4b). Consistent

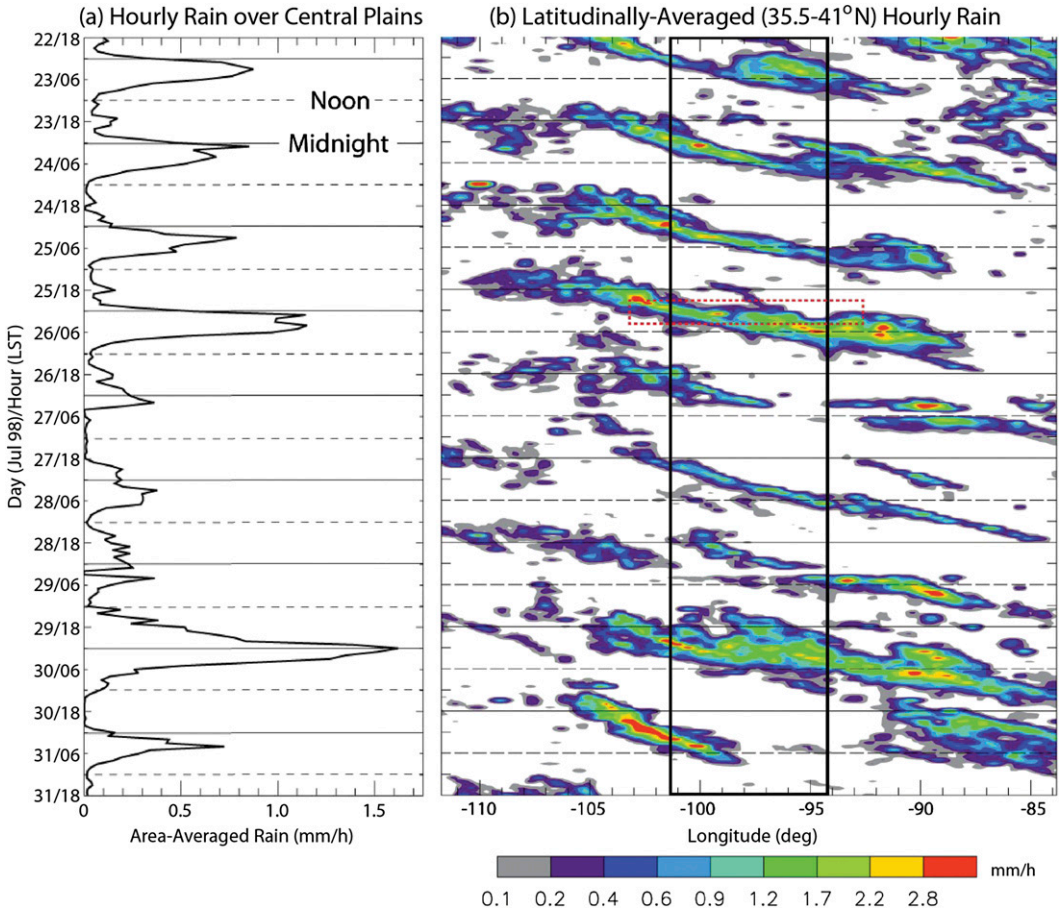

FIG. 2. (a) Time series of area-averaged Stage-4 hourly precipitation for the 600 km × 500 km westernmost rectangular region in Fig. 1a. (b) Time–longitude diagram of Stage-4 hourly rainfall averaged over the latitude band depicted by the vertical lines in Fig. 7a. The red dotted rectangle in (b) indicates the approximate spatiotemporal location of the radar reflectivity maps displayed in Fig. 3. The tall black rectangle in (b) indicates the longitudinal swath used for zonal averaging in (a) and in the time–latitude diagrams in Figs. 4 and 7.

with TD06, the two most intense area-averaged rain events occurring on 25–26 and 29–30 July (Fig. 2a) were associated with the strongest southerly LLJs (Fig. 4b).

The current corridor also shares some lower-tropospheric environmental features with heavy rainfall episodes of the East Asian mei-yu season including shallow fronts and strong LLJs. However, in the current case, there are pronounced differences in the relationship between the front and both the LLJ and precipitation. Here, the LLJ is oriented parallel to the frontal gradient (Fig. 4b) in contrast to Wang et al. (2014, their Fig. 2), who analyzed and simulated a period of heavy rainfall during the mei-yu season near Taiwan. The relationship between the LLJ and the front leads to primarily postfrontal precipitation, which also contrasts with the findings of Wang et al. (2014).

A ~2° southward shift in the corridor location near the middle of the 9-day period of the current case coincides with a decrease in the strength the 250-hPa zonal wind component at latitudes extending northward from the corridor's north edge (Fig. 4c). This marks the passage of a middle- to upper-tropospheric short-wave trough during which low 650-hPa relative humidities (located ~1–2 km above the PBL) become temporarily established in the northern part of the mean corridor region (Fig. 4d). During this time the frontal θ gradient weakens appreciably, resulting from subsidence-induced warming on the northern side of the baroclinic zone (Fig. 4b) implied by the strong decreases in relative humidity located a few kilometers above (cf. Fig. 4c). The temporary weakening of the lower-tropospheric θ gradient and the concurrent weakness of the nocturnal LLJ (Fig. 4b) imply a weakening of lower-tropospheric lifting in the baroclinic zone, which is consistent with the smaller area-averaged rainfalls from 26 through 29 July (Figs. 2a,b).

The region south of 38°N has less transient behavior. Throughout the entire 9-day period, the high

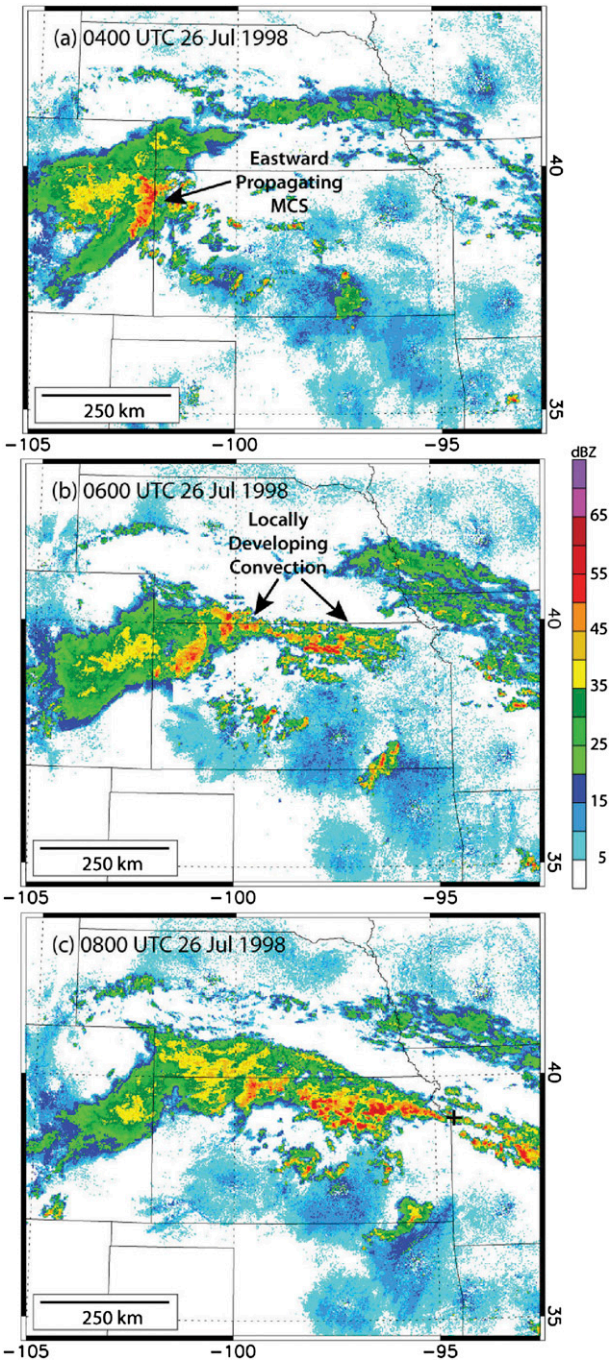

FIG. 3. Mosaics of Weather Surveillance Radar-1988 Doppler (WSR-88D) base-scan radar reflectivities at (a) 0400, (b) 0600, and (c) 0800 UTC 26 Jul 1998. The arrows in (a) and (b) denote precipitation features referred to in the text and the plus sign in (c) indicates the Kansas City, MO, metropolitan area. [The radar data used to construct these plots were obtained from the Iowa State University Department of Agronomy website (http://mesonet.agron.iastate.edu/archive).]

midtropospheric relative humidities within the corridor decrease substantially to its immediate south (Fig. 4d). This area lies within a transition zone between the weak-to-moderate westerlies in the corridor to weak easterlies farther south (Fig. 4c), consistent with the western edge of a 12-day mean upper-level anticyclone centered over the southern plains (Fig. 5a). The abrupt drop in MUCAPE over the southern plains from central Oklahoma through Texas (Fig. 1b) is partly influenced by the large-scale anticyclone (Fig. 5a), which is consistent with the composite corridor conditions of TD06.

3. Numerical model and experiment design

a. *Numerical model*

Each of our simulations (Table 1) uses version 3.4.1 of the Advanced Research core of the Weather Research and Forecasting (WRF) Model (ARW; Skamarock and Klemp 2008). Most of the simulations, including the control simulation (CONTROL), use a single 1000×565 horizontal domain with horizontal grid spacing of $\Delta = 3$ km. This domain covers the majority of the continental United States and is indicated by the dashed rectangle in Fig. 5a. The vertical grid contains 43 levels with a model top near 50 hPa and has enhanced resolution in the PBL, where $\Delta z < 100$ m through the lowest six model levels. Physical parameterizations include the Mellor–Yamada–Janjić (MYJ) PBL scheme (Janjić 2002), the WRF single-moment six-class (WSM6) bulk microphysical parameterization (Hong et al. 2004), and the Rapid Radiative Transfer Model (RRTM) longwave (Mlawer et al. 1997) and Dudhia (1989) shortwave radiation schemes. The ARW atmospheric model is coupled to the Noah land surface model (Chen and Dudhia 2001; Ek et al. 2003).

The model is integrated for 12 days from 0000 UTC 20 July to 0000 UTC 1 August 1998 and uses, unless otherwise specified, initial conditions and 3-h lateral boundary conditions (LBCs) obtained from National Centers for Environmental Prediction (NCEP) Eta Model analyses. As in our analysis of observations in section 2, we focus our analysis on the final 9 days of the simulations (0000 UTC 23 July–0000 UTC 1 August). This period corresponds to that during which the corridor location was most steady and allows 72 h for model spinup. Rather than analyzing the deterministic prediction of individual precipitation systems, the precipitation is diagnosed in terms of its statistical properties and those of related meteorological fields, which is most meaningful for simulations of this duration.

b. *Control simulation and sensitivity studies*

Our horizontal domain selection is largely dictated by the size at which the model can easily be run at

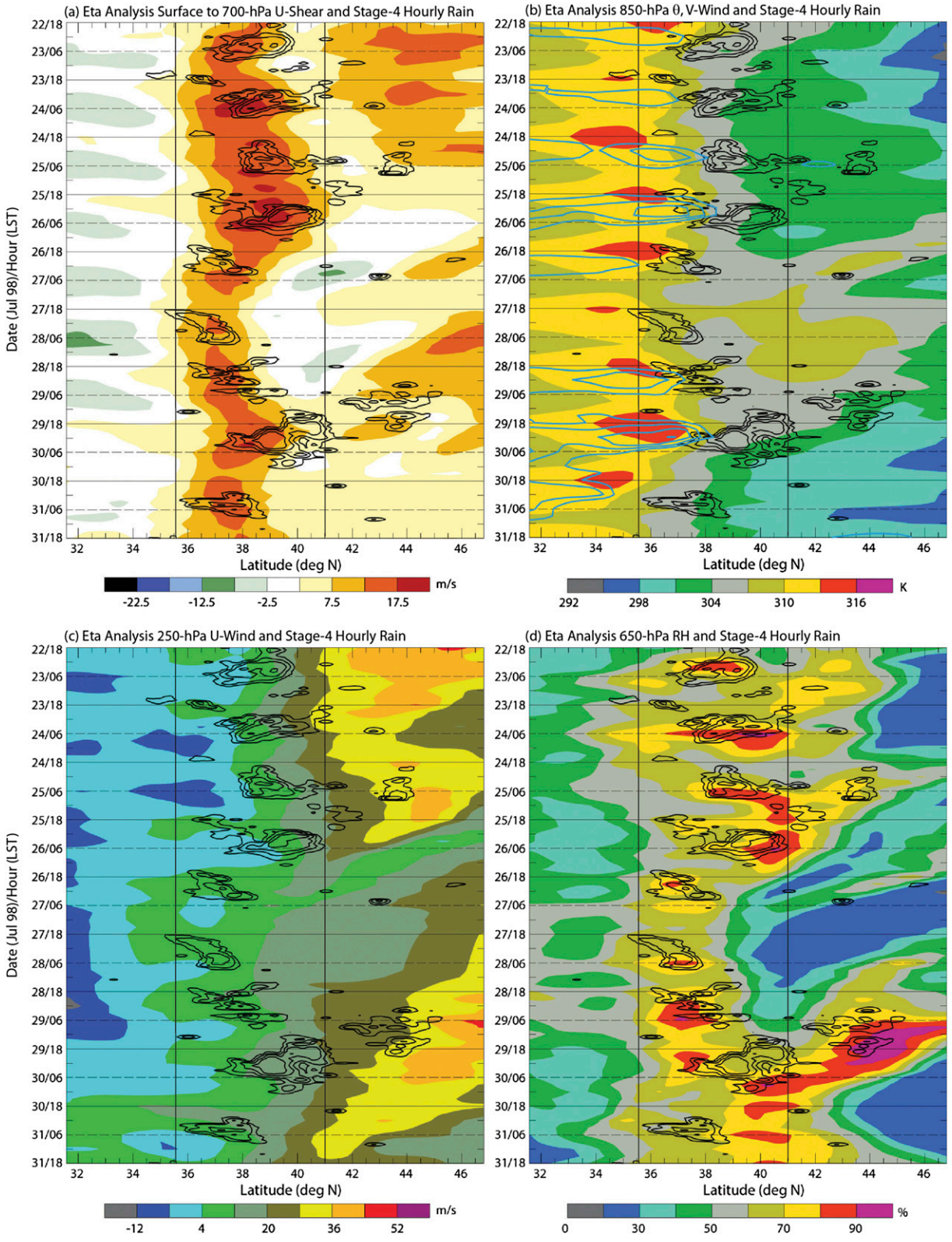

FIG. 4. Time–latitude diagrams of the (a) surface–700-hPa zonal wind difference, (b) 850-hPa potential temperature, (c) 250-hPa zonal wind, and (d) 650-hPa relative humidity from 3-hourly Eta Model analyses longitudinally averaged over the region indicated by the black vertical lines of the rectangle in Fig. 2b. The black contours in each panel indicate longitudinally averaged hourly rainfall from Stage-4 analyses exceeding 0.2, 0.6, 1.4, and 3 mm h^{-1} and the cyan contours in (b) indicate longitudinally averaged 850-hPa meridional wind speeds exceeding 7.5, 10, 12.5, and 15 m s^{-1} from 3 hourly Eta Model analyses.

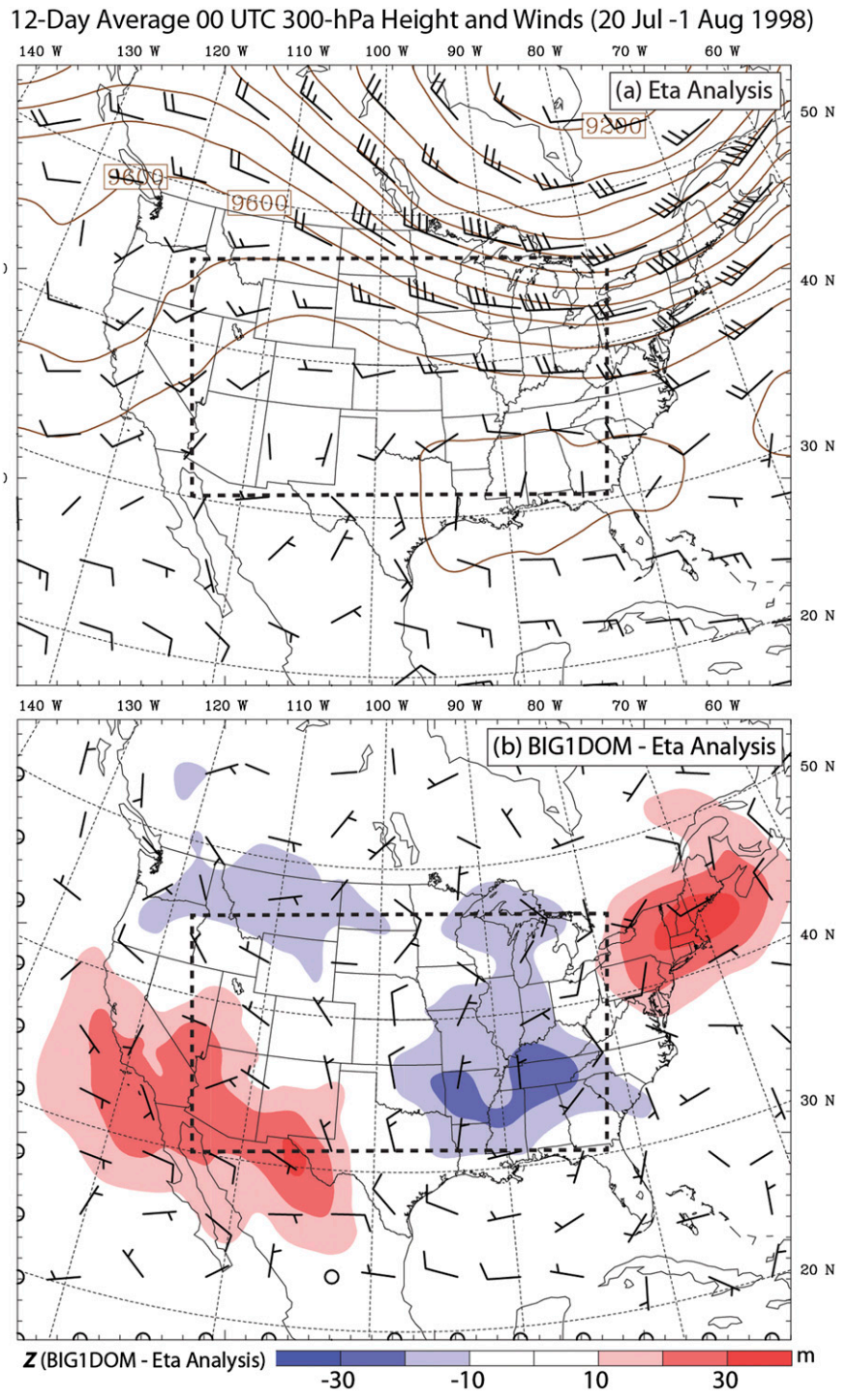

FIG. 5. Time-averaged 0000 UTC 300-hPa (a) geopotential heights (contour intervals of 50 m) and horizontal winds from the Eta Model analyses, and (b) geopotential height (color shading) and horizontal wind difference fields between BIG1DOM (used as lateral boundary conditions for NESTDOM) and the Eta Model analyses (used as lateral boundary conditions for CONTROL and other high-resolution simulations). The dashed inset in each panel indicates the location of the high-resolution domain.

TABLE 1. Listing of 288-h simulations from 0000 UTC 20 Jul to 0000 UTC 1 Aug 1998. Additional details are provided in the text.

Simulation	Domain	Convection	Initial conditions	Lateral BCs	Miscellaneous	Purpose
CONTROL	3000 km × 1695 km; $\Delta x,y$ = 3 km	Explicit	0000 UTC 20 Jul 1998 Eta analysis	Eta analysis Δt = 3 h		Compare with observations
CONSTSM	3000 km × 1695 km; $\Delta x,y$ = 3 km	Explicit	0000 UTC 20 Jul 1998 Eta analysis	Eta analysis Δt = 3 h	Time-invariant soil moisture	Test role of soil wetness changes
DIURNAL	3000 km × 1695 km; $\Delta x,y$ = 3 km	Explicit	0000 UTC Eta analysis (12-day average, 20 Jul–1 Aug)	Eta analysis, diurnal variation only, Δt = 3 h		Test role of transient disturbances
NESTDOM	3000 km × 1695 km; $\Delta x,y$ = 3 km	Explicit	0000 UTC 20 Jul 1998 Eta analysis	BIG1DOM run Δt = 3 h		Test role of large-scale forcing
BIG1DOM	5940 km × 4035 km; $\Delta x,y$ = 15 km	Teidtke cumulus	0000 UTC 20 Jul 1998 Eta analysis	Eta analysis Δt = 3 h		Test roles of domain size and explicit convection

"convection permitting" resolution, which while inadequate for resolving individual convective cells (Bryan et al. 2003), represents salient mesoscale aspects of the deep convection and obviates the need for cumulus parameterization. Recent refinements to observationally based composite studies (e.g., Maddox 1983; Cotton et al. 1989) on how MCSs interact with their mesoscale environment have come from studies using numerical models at similar convection-allowing resolutions (e.g., Trier et al. 2006; Tao et al. 2013).

The intermediate size of our domain also provides the strong constraint of more accurate large-scale forcing in its interior via 3-h analyses applied at the lateral boundaries. Inasmuch as the large-scale forcing is expected to have an important influence on the properties of long-lived heavy precipitation corridors, this domain configuration is anticipated to permit a more faithful simulation than what might be obtained using domain sizes and/or grid spacings typical of larger limited-area regional climate and operational numerical weather prediction (NWP) models.

The importance of these attributes is demonstrated with a simulation BIG1DOM, which uses a horizontal domain the size of the Eta analysis displayed in Fig. 5a with 370 × 297 horizontal grid points and a much coarser grid spacing of Δ = 15 km. Unlike in CONTROL and the remainder of the simulations to be discussed, this larger and coarser domain simulation requires a cumulus parameterization and here we use the Tiedtke (1989) scheme.

In the previous section we noted a closed anticyclone over the southeastern United States extending westward into the southern plains in the 12-day mean 300-hPa Eta analysis (Fig. 5a). The BIG1DOM − Eta analysis geopotential height differences for this period (Fig. 5b) indicate higher simulated heights over the southwestern United States and lower simulated heights extending from the upper Midwest into the lower Mississippi Valley. This results in perturbation upper-tropospheric northerlies throughout the plains and into Texas (Fig. 5b). Though the height and wind departures from the analyzed conditions are of relatively small amplitude, they are superposed onto a weak upper-level flow pattern (Fig. 5a) that is characteristic of warm-season heavy precipitation corridors (TD06) and are, thus, capable of changing the regional-scale height pattern and flow direction. Moreover, the largest anomalies are located near the western and southern boundaries of the high-resolution domain (dashed rectangle in Fig. 5) used in CONTROL and other simulations (Table 1).

The foregoing aspect of BIG1DOM motivates the NESTDOM simulation. NESTDOM tests the effects of differences in the mean regional-scale pattern that arise from degraded LBCs (including the misrepresentation of the mid- to upper-level anticyclone) on corridor simulations by using the convection-permitting domain of CONTROL. However, in NESTDOM the 3-h LBCs are supplied in a one-way nest from BIG1DOM instead of from the Eta analysis (Fig. 5a). Hence, the LBCs for the nest are derived similarly to those in CONTROL but deviate significantly from the Eta analysis and thus provide a measure of corridor robustness in the face of modest synoptic-scale flow changes.

Another external aspect that may influence corridor precipitation is transient synoptic disturbances including mid- to upper-tropospheric short waves. Specifically, midtropospheric drying (Fig. 4d) coincident with the passage of a disturbance in the upper-level westerlies (Fig. 4c) was associated with a temporary weakening (Fig. 2) and a ~2° southward shift of corridor precipitation (Fig. 4). We quantify the influence that similar transient disturbances moving through the lateral boundaries have on the precipitation in an additional

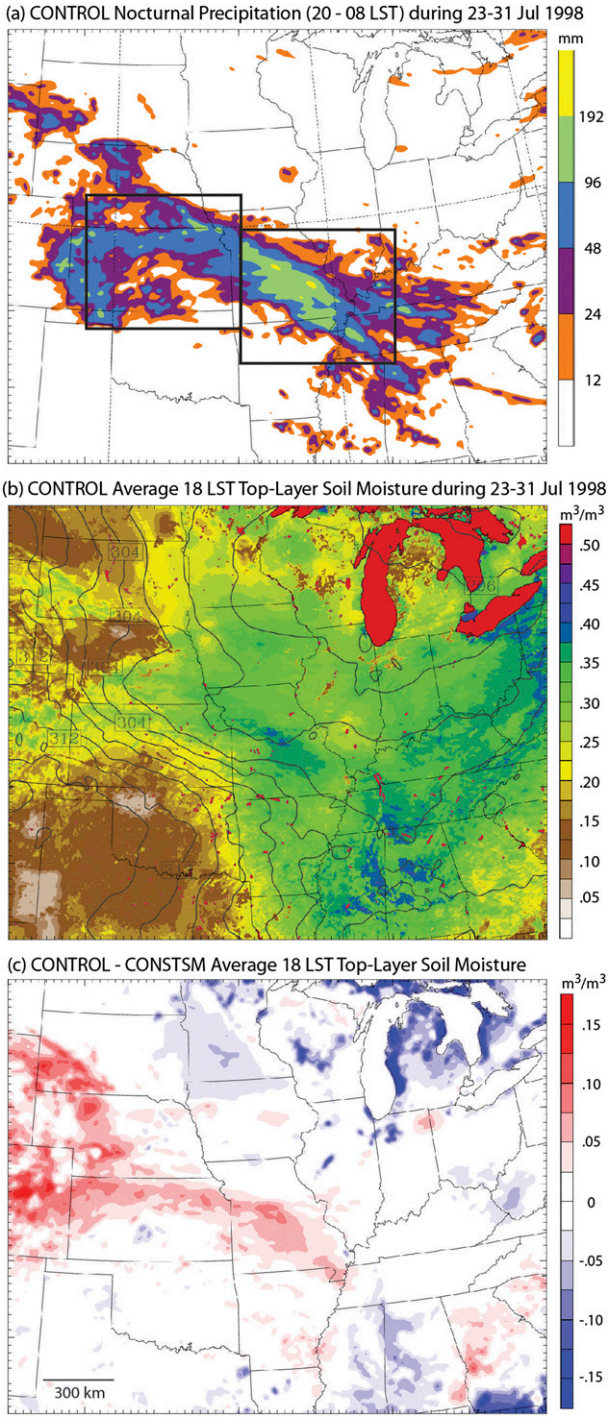

FIG. 6. (a) As in Fig. 1a, but for CONTROL. (b) The 9-day-averaged 0000 UTC volumetric soil moisture in the top 0.1 m and potential temperature (2-K contour intervals) at ~500 m AGL for CONTROL. (c) The 9-day-averaged 0000 UTC volumetric soil moisture difference field in the top 0.1 m between CONTROL and CONSTSM, which uses time-invariant soil moisture.

simulation, DIURNAL. DIURNAL is identical to CONTROL except that it specifies the LBCs to be diurnal averages from the 12-day simulation period that are provided at 3-h intervals, following Trier et al. (2010). Note that this simulation employs both a different set of initial conditions and different LBCs from those in CONTROL (Table 1). However, based on the work of Sun and Zhang (2012), who isolated these effects in separate simulations of heavy precipitation near East Asian mei-yu fronts, we anticipate the temporally periodic LBCs to have a more significant effect on the corridor than the time-averaged initial conditions during our 9-day analysis period beginning at $t = 72$ h.

Together, NESTDOM and DIURNAL are designed to examine the importance of the *external* influences of the large-scale pattern and transient disturbances, respectively, on the intensity, location, and persistence of the heavy precipitation corridor. However, the repeated local occurrence of precipitation (Fig. 2) may exert important *internal* controls on the corridor as well. One internal factor is the increase of soil moisture in the corridor. Figure 6c shows a positive departure of top-layer soil moisture in CONTROL from that of the initial conditions, which is spatially correlated with the 9-day nocturnal precipitation region across northern Kansas through central and southeastern Missouri (Fig. 6a).

The enhancements from the initial conditions represent a sizeable fraction (20%–30%) of the total soil moisture over much of northern Kansas (Fig. 6b). Moreover, the volumetric soil moisture values in this region (between 0.1 and 0.3 $m^3\,m^{-3}$) are typical of those that define transition zones between wet and dry climates, over which seasonal precipitation amounts can be particularly sensitive to soil moisture changes (e.g., Koster et al. 2004). Thus, we test the effects of soil moisture evolution on the precipitation and its environment in the CONSTSM simulation, which is identical to CONTROL except that the soil moisture is not allowed to vary temporally.

Here, no attempt is made in any of the simulations to provide "spunup" initial soil conditions (e.g., Chen et al. 2007), which have been used in previous simulations of similar duration (e.g., Trier et al. 2008). Our simple approach is motivated by the desire to have the same initial soil conditions for the entire set of sensitivity experiments, of which some (most notably DIURNAL) employ significant idealizations to the atmosphere.

4. Diurnal cycle of simulated precipitation in the corridor

To provide a concise overview of the five simulations, we construct diurnal frequency diagrams in which, for

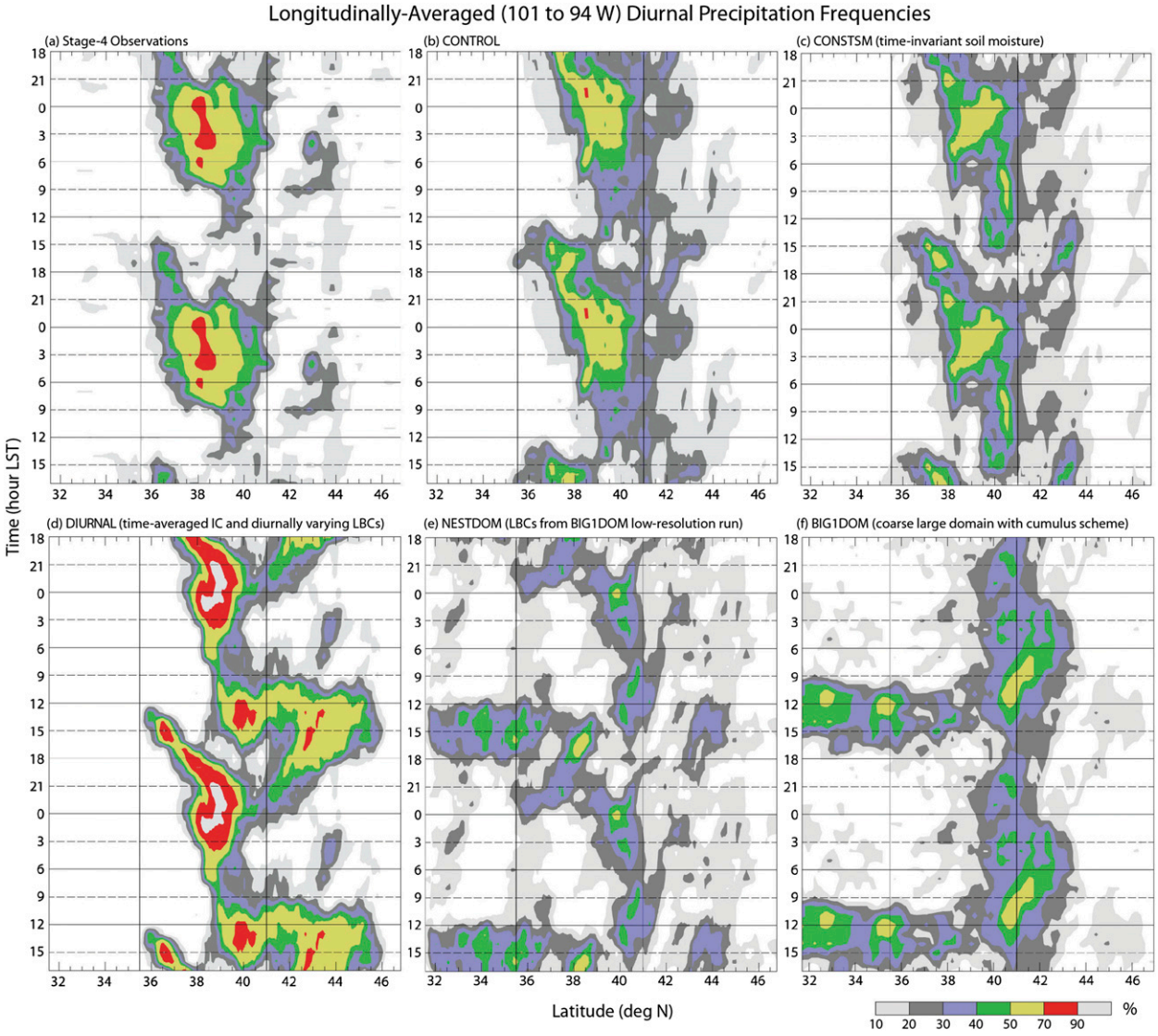

FIG. 7. Time–latitude diurnal frequency diagrams of precipitation exceeding 0.1 mm h^{-1} for horizontal averages over a 600-km zone (~−101° to −94° longitude) indicated by the solid black vertical lines in Fig. 9 during the 9-day period from 23 through 31 Jul 1998 from (a) Stage-4 analyses, and simulations (b) CONTROL, (c) CONSTSM, (d) DIURNAL, (e) NESTDOM, and (f) BIG1DOM. The black vertical lines indicate the broadly defined corridor region.

a given threshold, the exceedance frequency of longitudinally or latitudinally averaged rainfall is plotted as a function of time or day and the nonaveraged spatial coordinate. Following Carbone et al. (2002), we choose a threshold of 0.1 mm h^{-1}, which constitutes averages over 600-km swaths of either longitude or latitude. Exceedance of this relatively low threshold indicates when and where it rains. Information from these frequency diagrams is then supplemented by area-averaged rain amounts over similar dimensions.

Figure 7 presents time–latitude rainfall frequency diagrams averaged through the longitude band indicated by the black vertical lines in Fig. 2b and the westernmost rectangles in Figs. 1a and 6a. This constitutes the region where both the observed near-surface front (Fig. 1b) and that simulated in CONTROL (Fig. 6b) are strongest. The observed latitudinal corridor is evident between ~37° and 40°N with a striking nocturnal coherence beginning during late evening and lasting overnight (Fig. 7a). The latitudinal placement of the corridor in CONTROL (Fig. 7b) agrees well with the observations (Fig. 7a). The frequencies are also similar, though CONTROL has decreased coverage of the highest frequencies (70%–90%), and its nocturnal corridor begins and ends ~2–3 h earlier than observed. These differences manifest themselves in differences in both the

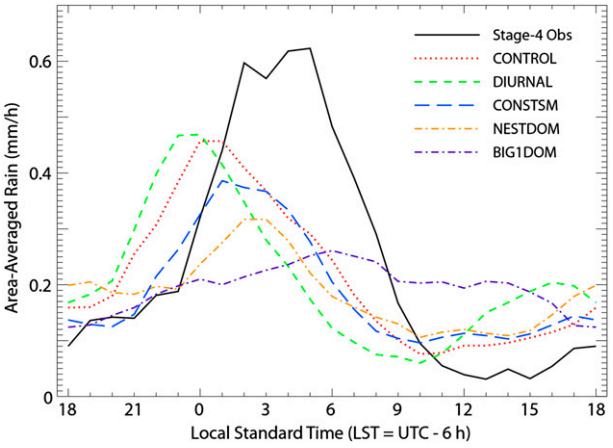

FIG. 8. Area-averaged hourly precipitation over the 600 km × 500 km regions denoted by the westernmost rectangles in Figs. 1a and 6a during the 9-day period from 23 to 31 Jul 1998. For simulation BIG1DOM, the centroid of the averaging region is shifted 150 km farther north to accommodate differences in corridor locations (cf. Fig. 7f).

intensity and timing of peak area-averaged rainfall amounts within the corridor between CONTROL and the Stage-4 analyses (Fig. 8).

The meridional rainfall frequency diagram of CONSTSM (Fig. 7c) bears a strong resemblance to that of CONTROL (Fig. 7b), indicating that the evolution of soil moisture in CONTROL has limited effect on the overall corridor location and diurnal cycle. However, examination of area-averaged rainfall reveals smaller amounts during the first half of the nocturnal rains in the western part of the corridor for CONSTSM (Fig. 8), which contribute to an average daily total in this region that is ~13% less than in CONTROL (Table 2). This may be partly related to area-averaged relative humidities at $z \sim 500$ m AGL that are 2%–3% lower in CONSTSM than CONTROL in the early evening, which could enhance subcloud rainfall evaporation and temporarily limit precipitation amounts reaching the ground. Though subcloud relative humidities increase as the evening PBL cools, the earlier convection initiation in CONTROL could conceivably influence subsequent MCS evolution and area-averaged precipitation amounts, which do not become comparable in CONTROL and CONSTSM until after midnight (Fig. 8).

The timing and location of the nocturnal corridor in DIURNAL (Fig. 7d) is similar to that of CONTROL but has significantly larger frequencies. This aspect is consistent with the temporally periodic LBCs chosen for the simulation (section 3b). Though the frequencies in the corridor are much greater in DIURNAL, area-averaged rainfall amounts are very similar to CONTROL (Fig. 8, Table 2). This results from the DIURNAL corridor rainfall being more regular and concentrated (which increases spatial coherence) but no more intense than in CONTROL, which is similar to results obtained by Sun and Zhang (2012) in their simulations of mei-yu fronts. Another high-frequency feature in DIURNAL is afternoon convection centered near 42°–46°N. Note that this has the effect of expanding the latitudinal zone of significant overall precipitation (Fig. 7d) from that observed (Fig. 7a) and simulated in CONTROL (Fig. 7b).

The NESTDOM Simulation demonstrates that the use of convection-permitting grid spacing alone provides no guarantee that a corridor will be accurately simulated. Here, nocturnal rainfall in the corridor is shifted northward and occurs less frequently (Fig. 7e), while unlike in the observations (Fig. 7a) and any of the other high-resolution simulations (Figs. 7b–d) daytime precipitation south of the corridor occurs on about 30%–60% of the days. The overall pattern of the NESTDOM diurnal frequency diagram appears most similar to that of BIG1DOM (Fig. 7e), which is not surprising since NESTDOM uses LBCs from BIG1DOM. The large frequencies of daytime precipitation south of the corridor region in NESTDOM and BIG1DOM (which are absent in the observations and other simulations) are primarily due to departures of the large-scale flow in these two simulations from that of the Eta analyses and are discussed in section 6b.

The BIG1DOM corridor of highest precipitation frequencies (near 41°N) is located even farther north than for NESTDOM. Even accounting for meridional differences in corridor location, BIG1DOM has the weakest diurnal cycle of area-averaged precipitation amounts of any of the simulations (Fig. 8).

The observed nocturnal precipitation corridor extends significantly beyond the eastern boundary of the western rectangle in Figs. 1a and 6a. Significant eastward increases in daily average precipitation occur for all simulations (Table 2) in the area delineated by the eastern rectangle. For example, there is a 69% increase in this eastern part of the corridor in CONTROL, even though the strength of the surface front is somewhat weaker than farther west (Fig. 6b). These regional precipitation increases in CONTROL are supported by corresponding ~10% increases in daily averaged CAPE and precipitable water over the southeast part of the corridor (not shown). However, the eastward increase in precipitation is only about 15% in the observations (Table 2).

Time–longitude rainfall frequency diagrams (Fig. 9) averaged for 600 km between the vertical lines in Fig. 7 reveal possible reasons for the differences between the observations and the simulations in the eastern part of the corridor. Both the Stage-4 radar analyses (Fig. 9a) and CONTROL (Fig. 9c) exhibit a coherent eastward-propagating signal of enhanced rainfall frequencies that emanate from

TABLE 2. 9-day (23–31 Jul) area-averaged rainfall (mm day^{-1}) over the western (second column) and eastern (third column) corridor regions indicated by the two sets of rectangles in Figs. 1a and 6a, and for the high-resolution model domain indicated by dashed rectangles in Fig. 5, excluding the 50 grid points closest to the lateral boundaries (fourth column). Note that the rectangles (Figs. 1a and 6a) used for the corridor averages of BIG1DOM have been shifted northward by 90 km from those used for the Stage-4 analyses and the other simulations to accommodate the more northward location of the corridor in this simulation (cf. Fig. 7e).

Simulation/observation	West corridor (600 km × 500 km)	East corridor (600 × 500 km)	Domain wide (2750 km × 1445 km)
Stage-4 obs	6.75	7.73	2.90
CONTROL	6.12	10.35	3.42
CONSTSM	5.36	10.13	3.33
DIURNAL	6.12	10.39	4.47
NESTDOM	4.53	9.01	3.12
BIG1DOM	5.53	9.12	3.55

the lee of the Rockies (−105°) during the afternoon and early evening and traverse the plains (−101° to −94°) overnight. This rainfall continues to propagate east of −94° in CONTROL, which also has a high frequency of daytime precipitation in the −94° to −88° longitude belt (Fig. 9c) that is largely absent from the observations (Fig. 9a) and accounts for the simulated excess (Table 2).

In a climatological sense this central Mississippi River valley region has a diurnal signal of weaker amplitude than does the plains area farther west (Carbone and Tuttle 2008), since it supports both decaying nocturnal convection moving through around sunrise and local regeneration following peak daytime heating. One possible reason for the departure from the climatological condition of frequent afternoon regeneration is the exceptionally high frequency of nocturnal convection that does not subside in the region until nearly midday and has strong stabilizing effects in its wake. In CONTROL, the coherent eastward-propagating nocturnal signal is somewhat weaker and enters the region (−94°) several hours earlier (Fig. 9c), which might allow greater daytime recovery supporting afternoon convection.

Similar to other simulations that rely on cumulus parameterization in Davis et al. (2003), BIG1DOM has no eastward-propagating convection emanating from the Rockies (Fig. 9b). In addition, the convection originating from the Rockies in BIG1DOM begins several hours before the explicit deep convection in CONTROL (Fig. 9c) and up to 6 h before the peak of the observed stationary mountain convection (Fig. 9a). BIG1DOM also has moderate frequencies in the eastern corridor region (−94° to −88°), where precipitation occurs at almost any time of day. NESTDOM has eastward propagation emanating from the Rockies (Fig. 9d). However, the signal is considerably weaker than in CONTROL (Fig. 9c), suggesting the lack of propagation in BIG1DOM is affected not only by cumulus parameterization but also by other factors.

5. Physical processes influencing the diurnal cycle of corridor precipitation

In this section we examine factors that determine the location of deep convection in the corridor and its diurnal cycle. We focus on the western corridor region, marked by the white vertical lines in Fig. 10, since this ~−101° to −94° longitude band is where much of the nocturnal corridor precipitation both originates and is most accurately simulated in CONTROL (section 4).

The western half of the heavy nocturnal precipitation in the corridor lies within a narrow latitudinal zone where the 9-day-averaged 0100 LST minimum buoyancies of the most unstable (i.e., highest θ_e) parcel, which we refer to as $B_{\min}$,[1] have smaller magnitudes than over surrounding areas to the north and south (Fig. 10). Here, we use $B_{\min}$ as a surrogate for the convective inhibition (CIN) since $B_{\min}$, discussed further in Trier et al. (2014a), has the desirable property of spatial continuity. At the edge of the lower-tropospheric front marked by the shift from southerly to easterly winds, $B_{\min}$ has unfavorable 9-day-mean values from about −5° to −6°C, which increase to more favorable mean values from −2° to −3°C near the southern edge of the precipitation located 200–300 km to the north (Fig. 10).

Figure 11 displays the mean 9-day diurnal cycle of thermodynamic parameters at various distances (indicated by the color circles in Fig. 10) from the CONTROL nocturnal precipitation band. The location supporting corridor convection (black dot in Fig. 10) has relatively modest values of MUCAPE compared to locations farther south, where maximum values are found during late afternoon ~150 km from the rain corridor (Fig. 11a). However, at the location only ~50 km from the rain corridor, which is well north of

[1] Trier et al. (2014a) define $B_{\min}$ more generally as the minimum buoyancy (in temperature units) for an air parcel lifted from any specified level, not necessarily the level of highest equivalent potential temperature.

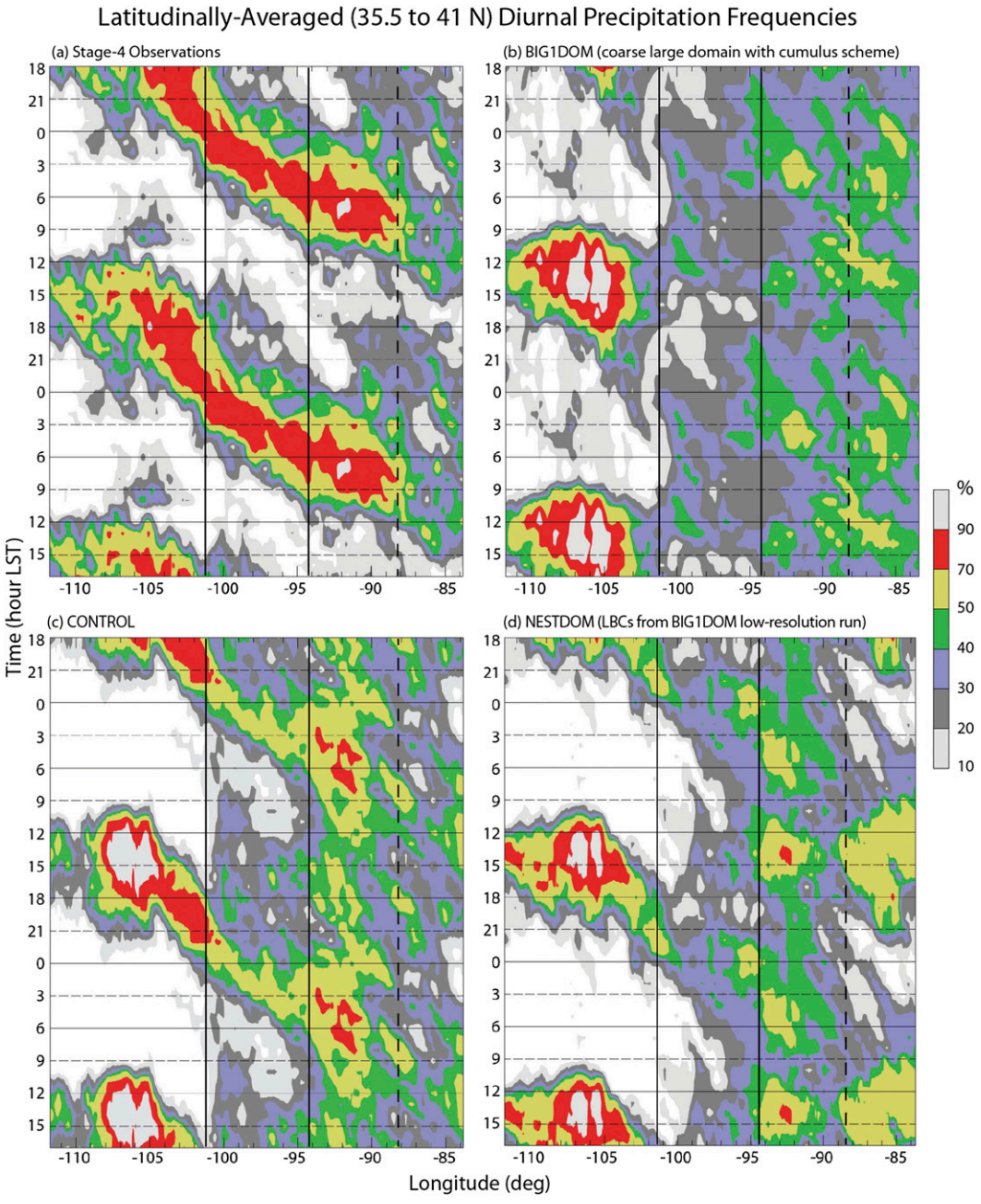

FIG. 9. Time–longitude diurnal frequency diagrams of precipitation exceeding 0.1 mm h^{-1} for horizontal averages over a 600-km zone (~35.5° to 41° latitude) indicated by the black vertical lines in Fig. 7 during the 9-day period from 23 through 31 Jul 1998 from (a) Stage-4 analyses, and simulations (b) BIG1DOM, (c) CONTROL, and (d) NESTDOM. The two sets of black vertical lines enclose longitudes that compose the western and eastern rectangular areas in Figs. 1a and 6b and the different sectors in the leftmost two columns of Table 2.

the surface front (Fig. 10), the magnitudes of CIN (Fig. 11b) for conditionally unstable air parcels are typically smaller and the relative humidities (Fig. 11d) above them are greater, which favors widespread deep convection.

This northernmost location close to the precipitation corridor has both late afternoon and overnight peaks of mean MUCAPE (Fig. 11a) with accompanying small CIN magnitudes (Fig. 11b). An important difference between these two times is that the height of the most unstable parcel is situated well above the surface at night (Fig. 11c). In contrast with daytime conditions where near-surface parcels have the largest CAPE, even smaller

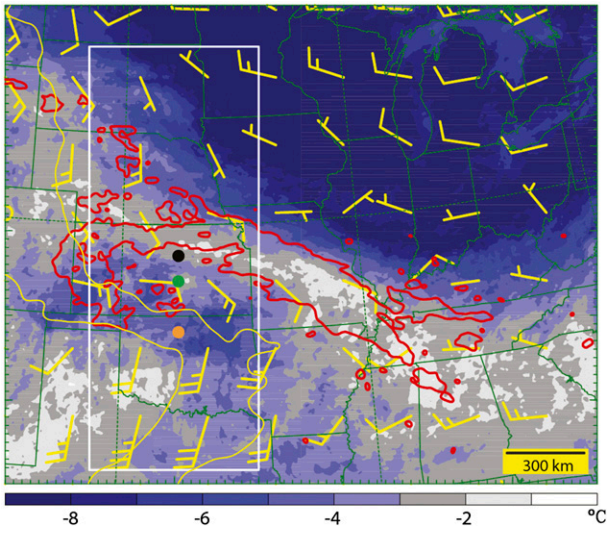

FIG. 10. 9-day averages (23–31 Jul 1998) of the minimum buoyancy (in temperature units) for the highest–equivalent potential temperature air parcels and horizontal winds at model level 5 (~400 m AGL) at 0100 LST for CONTROL with the position of simulated 9-day total rainfall from 2000 to 0800 LST exceeding 48 mm, indicated by the single red contour. The thin yellow contours indicate the 0100 LST 9-day-averaged positions of the 310- and 314-K isentropes, marking the approximate leading edge of the surface front in the western corridor region. The color-coded filled circles denote the positions of the 9-day time-averaged thermodynamic parameters displayed in Fig. 11. The white rectangle indicates the location of the x-averaged cross sections displayed in Figs. 12 and 13.

magnitudes of CIN are situated in a layer above the most unstable parcel at night (not shown). This is a common property of simulated MCS environments characterized by strong frontal lifting (Trier et al. 2014b).

Frontal lifting is evident in longitudinally averaged cross sections oriented approximately normal to the mean heavy precipitation corridor orientation, and is associated with the interaction of the nocturnal LLJ with the front (Fig. 12). In CONTROL the precipitation corridor begins near the terminus of the sloping LLJ (Fig. 12b) several hundreds of kilometers north of the leading edge of the surface front in a manner similar to that documented in an observationally based case study of an MCS (Trier and Parsons 1993), which occurred during the 3–4 June 1985 corridor of successive MCSs (e.g., Stumpf et al. 1991; Fortune et al. 1992; Smull and Augustine 1993).

The temporally periodic LBCs used in DIURNAL support especially strong coherence and separation of the precipitation corridor (which is marked by deep ascent) from the several hundred kilometers wide zone of weaker and shallower lifting between the southern frontal edge and where the corridor precipitation begins (x = 350–650 km in Fig. 12c). Evidence of the upward parcel displacements from mesoscale lifting are seen in the contours of the constant mixing ratio that tilt upward along the axis of the LLJ approximately parallel to the isentropes in the 1–4-km layer from x = 450 to 650 km (Fig. 12d).

Organized upward motion within the nocturnal corridor region during the afternoon in DIURNAL is both weaker than overnight and confined to a region in close proximity to the leading edge of the front (Fig. 13a). A similar situation occurs in CONTROL (not shown) but the front is less stationary, which contributes to more diffuse average daytime vertical motions than in DIURNAL. Although some late-afternoon convection is evident at this location south of the main nocturnal corridor in the observations (Fig. 7a) and simulations (Figs. 7b–d), dry air above the PBL in this location in CONTROL (e.g., Fig. 11d, gold curve) is deleterious to the formation of strong, long-lived deep convection (e.g., James and Markowski 2010). In this situation, conditions are much more favorable at night after the hot, but relatively dry, air originating south of the front has undergone substantial vertical displacements while being transported northward by the LLJ.

6. Factors influencing corridor location, intensity, and persistence

a. Influence of environmental conditions on the CONTROL precipitation corridor

Though individual precipitation events are not expected to correspond to observed ones in simulations having the duration of CONTROL, the overall relationships between the simulated precipitation events and environmental conditions in CONTROL (Fig. 14) are quite similar to observed ones (cf. Fig. 4) discussed earlier in section 2. These similarities include 1) heavy nightly precipitation events at the nearly stationary latitude of the strongest 850-hPa meridional θ gradients (Fig. 14b) and associated lower-tropospheric zonal vertical wind shear (Fig. 14a), 2) a 2–3-day interlude (26–28 July) of weaker precipitation events within the latitudinal corridor after a transient upper-air disturbance preceding weaker 250-hPa westerlies passes along the corridor's northern fringe (Fig. 14c) with corresponding lower midtropospheric relative humidities (Fig. 14d) and a concurrent temporary weakening of both the 850-hPa θ gradient and nocturnal LLJ (Fig. 14b), and 3) confinement of the heaviest rain to the latitudes where 650-hPa relative humidities, themselves located ~3 km AGL and 0.5–2.0 km above the PBL top, are highest (Fig. 14d).

One difference between the observations and CONTROL is that corridor relative humidities at this

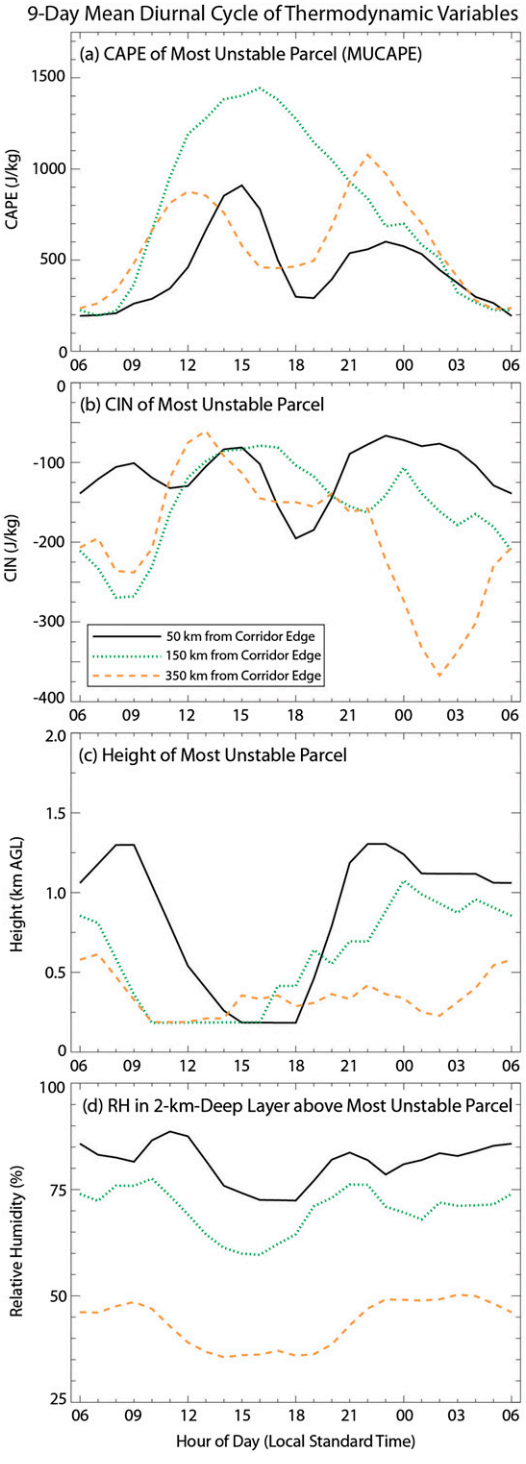

FIG. 11. Diurnal cycle of 9-day-averaged (23–31 Jul 1998) thermodynamic parameters at the locations of the corresponding color-coded solid circles in Fig. 10 for CONTROL. Shown are (a) CAPE, (b) CIN, and (c) height of the most unstable (highest θ_e) parcel, and (d) averaged relative humidity in the 2-km layer located immediately above the most unstable parcel. Each of the parcel thermodynamic quantities in (a)–(c) is calculated for a 50-hPa-deep-averaged parcel centered at the location of maximum θ_e.

level are typically 10%–20% greater in CONTROL (cf. Figs. 4d and 14d). The reasons for this discrepancy are not obvious. However, these differences may influence the simulated 2–3-h earlier than observed onset of evening precipitation within the portion of the corridor located over the same longitude band (Fig. 8). Support for this notion comes from a climatological study conducted over the southern plains, where Zhang and Klein (2010) related the timing of deep convection initiation to relative humidity values above the PBL.

Figure 15a indicates that maximum MUCAPE typically resides within the latitudinal corridor of heavy precipitation. However, the location of maximum midtropospheric relative humidity within the corridor shows less spatial variability than MUCAPE (cf. Figs. 15a and 14d). Moreover, when occasional extrusions of heavy precipitation in CONTROL occur to the north of the latitudinal corridor in advance of transient disturbances, they are more often associated with large 650-hPa relative humidities (Fig. 14d) than with especially large MUCAPE (Fig. 15a). To the south of the corridor, limited MUCAPE and low midtropospheric relative humidities continually conspire to make conditions unfavorable for organized heavy precipitation. There, MUCAPE becomes less favorable during the simulation (Fig. 15a), which is not uncommon under long-lived anticyclonic mid- and upper-tropospheric conditions (Fig. 5a).

b. *Comparison of CONTROL with sensitivity studies*

Both the patterns of precipitation and MUCAPE in and near the corridor are quite similar in CONSTSM (Fig. 15c) to their counterparts in CONTROL (Fig. 15a). In DIURNAL regular nightly events mature in approximately the same location within the 38°–40°N band (Fig. 15d) leading to exceptionally large coherence in diurnal frequencies (Fig. 7d). However, as noted in section 4, the area-averaged rain within the broadly defined corridor of observed events (Fig. 1a, western rectangle) was approximately the same as in CONTROL (Fig. 8, Table 2). This is partly a consequence of DIURNAL having less daily variability and thus lacking the few extreme area-averaged rain events that preceded transient disturbances including 25–26 and 29–30 July from the observations (Fig. 2a) and analogs from CONTROL (not shown).

An obvious difference between DIURNAL and the other simulations conducted over the high-resolution domains is frequent large MUCAPE extending well north of the observed corridor region (Fig. 15d). This is consistent with a lack of thermodynamic stabilization that occurs in the subsiding phase of translating transient disturbances, which are largely mitigated in DIURNAL by the temporally periodic LBCs. Here, in addition to the nightly corridor rainfall, there was also frequent

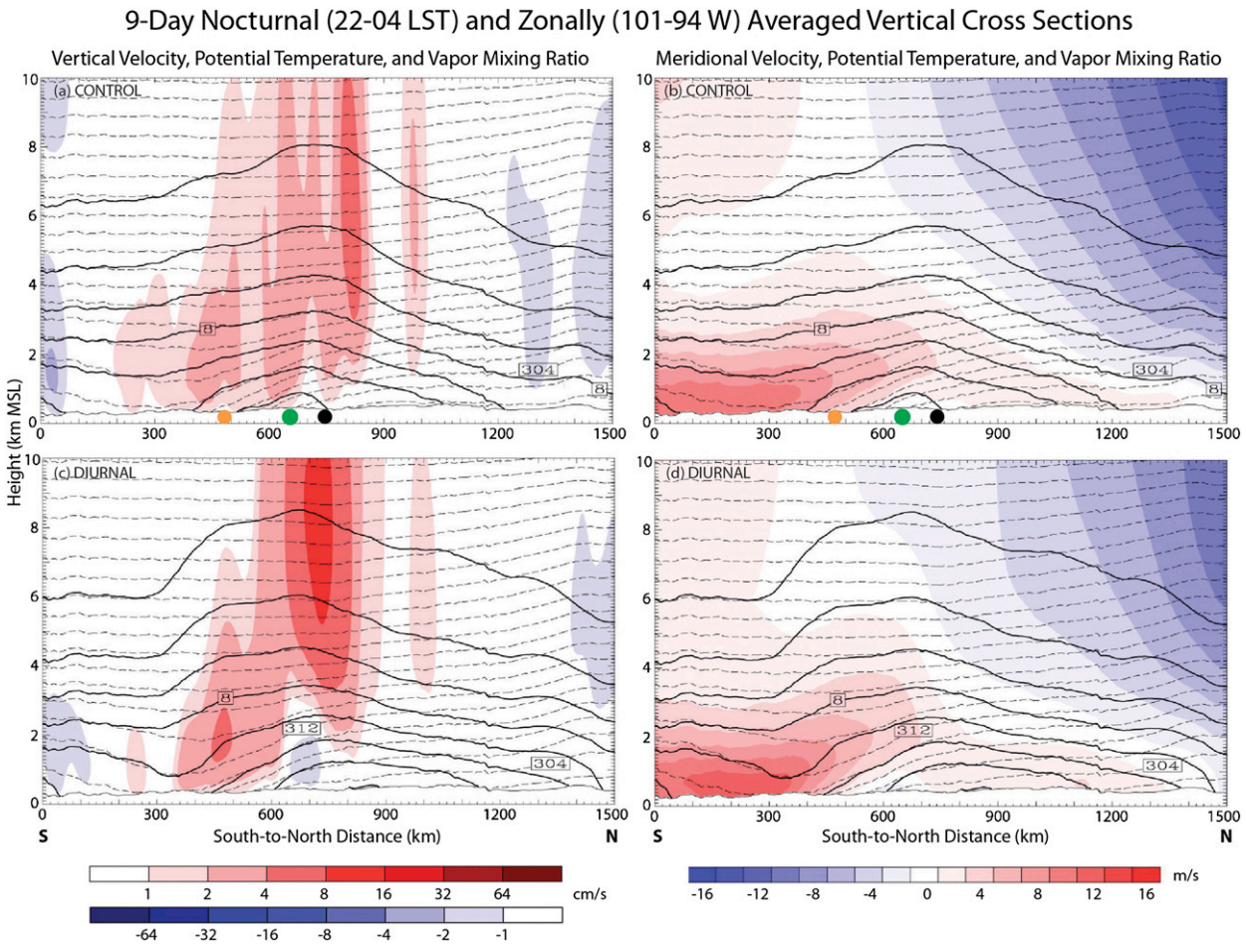

FIG. 12. Temporally averaged nocturnal vertical cross sections, which are also zonally averaged across the region indicated by the white rectangle in Fig. 10. Potential temperature (dashed lines, 2-K contour intervals), water vapor mixing ratio (solid lines, 2 g kg^{-1} contour intervals), and (a),(c) vertical velocity and (b),(d) meridional wind components for (top) CONTROL and (bottom) DIURNAL. The color-coded solid circles in the top panels indicate the meridional locations (Fig. 10) of the 9-day-averaged thermodynamic parameters in Fig. 11, which unlike the cross sections in the current figure, are not zonally averaged.

triggering of afternoon convection within the 42°–46° latitude band (cf. Fig. 7d) of moderate-to-large MUCAPE near the Black Hills of South Dakota. This convection was also long lived and had subsequent southeastward propagation (Fig. 15d). This aspect of DIURNAL, which had no analog in the observations, contributed to significantly greater domain-averaged daily rainfalls in DIURNAL than in any of the other simulations (Table 2). Thus, one may infer that weak transient disturbances, in addition to a favorable nearly stationary large-scale flow, are needed to maintain a narrowly confined rainfall region. Furthermore, the net effect of the transients is to reduce, rather than enhance, the total rainfall.

Over the 35.5°–41°-latitude heavy precipitation corridor, NESTDOM has the largest departures from CONTROL of any of the high-resolution sensitivity simulations (cf. Figs. 7b,e). Differences between these two simulations begin early in the analysis period and last through the entire simulation. The NESTDOM (Fig. 15b) corridor has more systematic southward nightly shifts in the position of precipitation and a longer and a more pronounced interlude of reduced precipitation (25–28 July).

Cooling related to precipitation reinforces the lower-tropospheric baroclinic zone and helps define its leading edge. This is evident from the southward progression of the 850-hPa θ gradient coinciding with the location of precipitation in NESTDOM (Fig. 16a), which by contrast remains quasi-stationary in CONTROL (Fig. 14b). The systematic southward nightly shift of precipitation in NESTDOM is made possible by larger MUCAPE (Fig. 15b) and midtropospheric relative humidities (Fig. 16b) south of the corridor than those found in CONTROL (Figs. 15a and 14d). Much stronger midtropospheric drying is associated with the 25–28 July period of more

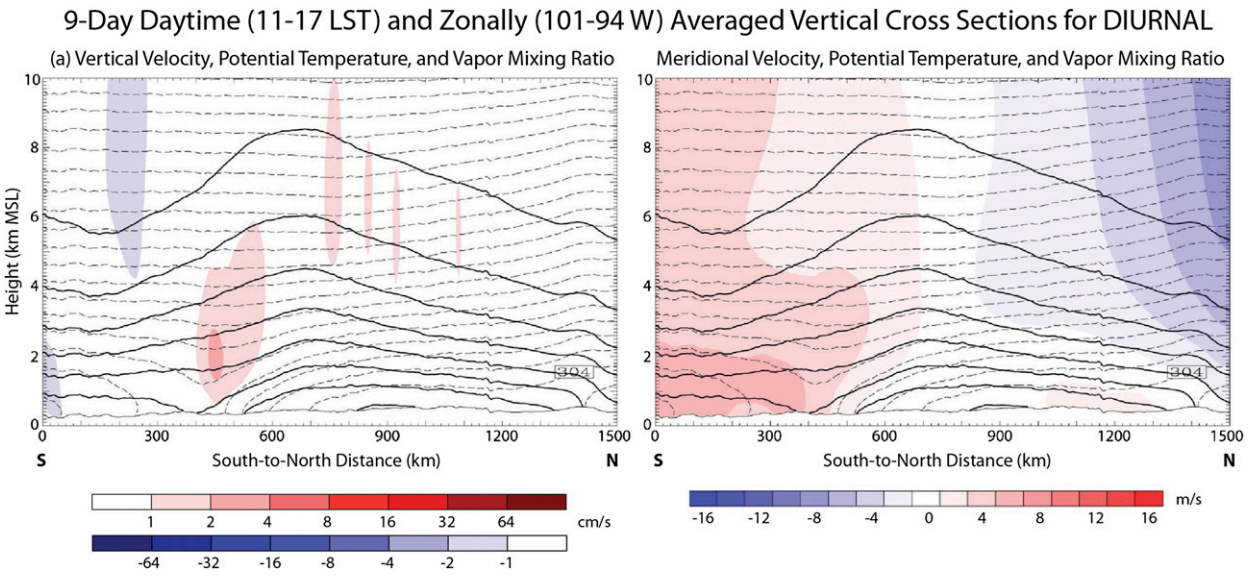

FIG. 13. As in Fig. 12c,d, but for daytime (1100–1700 LST) 9-day averages.

appreciable precipitation reduction than in CONTROL (cf. Fig. 16b with Fig. 14d). In NESTDOM, unlike in CONTROL, the midtropospheric drying also penetrates southward well beyond the latitudinal boundaries of the corridor.

Recall from section 2 that CONTROL and NESTDOM are performed identically in the same high-resolution domain except for the LBCs, where CONTROL is forced by the Eta analysis and NESTDOM is forced by output from the coarser-resolution simulation BIG1DOM performed over the Eta analysis domain. By examining the differences between the Eta analysis and BIG1DOM in the evolution of θ and winds on the 2–potential vorticity unit (PVU; 1 PVU $= 10^{-6}\,\mathrm{m^2\,K^{-1}\,s^{-1}}$) dynamic tropopause (Fig. 17), we are able to obtain insights into the reasons for differences between NESTDOM and CONTROL related to differences in the external forcing.

Important differences are evident by $t = 96$ h (1800 LST 23 July from $-101°$ to $-94°$ longitude) near the southern boundary of the high-resolution domain (dashed inset), where a deep cold-core cyclone extends from New Mexico into west Texas in BIG1DOM (Fig. 17b) but is much less well developed in the Eta analysis (Fig. 17a). As a result, upper-level westerly flow constitutes the southern LBC (Fig. 17b) for NESTDOM compared to upper-level southerly flow south of the precipitation corridor (Fig. 17a) for CONTROL. During the next 2 days the circulation on the east side of this vortex in BIG1DOM contributed to the enhanced MUCAPE (Fig. 15b) and midtropospheric relative humidities (Fig. 16b) south of the corridor that favored the nightly southward progression of convection in NESTDOM. Note that the more anticyclonic upper-level conditions influencing CONTROL at its southern boundary indirectly result in a stronger and more stationary precipitation corridor by making conditions less favorable to its south.

Another difference at $t = 96$ h includes greater θ and a related stronger anticyclone over the west in the Eta analysis (Fig. 17a) than in BIG1DOM (Fig. 17b). The establishment of a stronger ridge in the Eta analysis in this location diverted the northwesterly flow intruding into the high-resolution domain from Canada toward the upper Midwest several days later (Fig. 17c). In contrast, the upper-level northwesterly winds intrude into the high-resolution domain at a more western longitude and reinforce the flow behind the weakening vortex at more southern latitudes leading to a strong northerly component over the plains at all latitudes in BIG1DOM (Fig. 17d).

These two separate differences between the Eta analysis and BIG1DOM beginning early in the simulation period are the primary factors leading to the time-averaged differences displayed earlier in Fig. 5b. There, the time-averaged higher-amplitude upper-level pattern in BIG1DOM associated with a perturbation trough (ridge) in the Mississippi valley (southwest) leads to a more northerly component over the plains. Consistent with the climatological results of TD06, the much weaker LLJs in NESTDOM (Fig. 16a) than in CONTROL (Fig. 14b) are associated with boundary forcing of stronger upper-tropospheric northerlies over the plains (Fig. 5b), and are an additional factor contributing to the weaker precipitation corridor in NESTDOM.

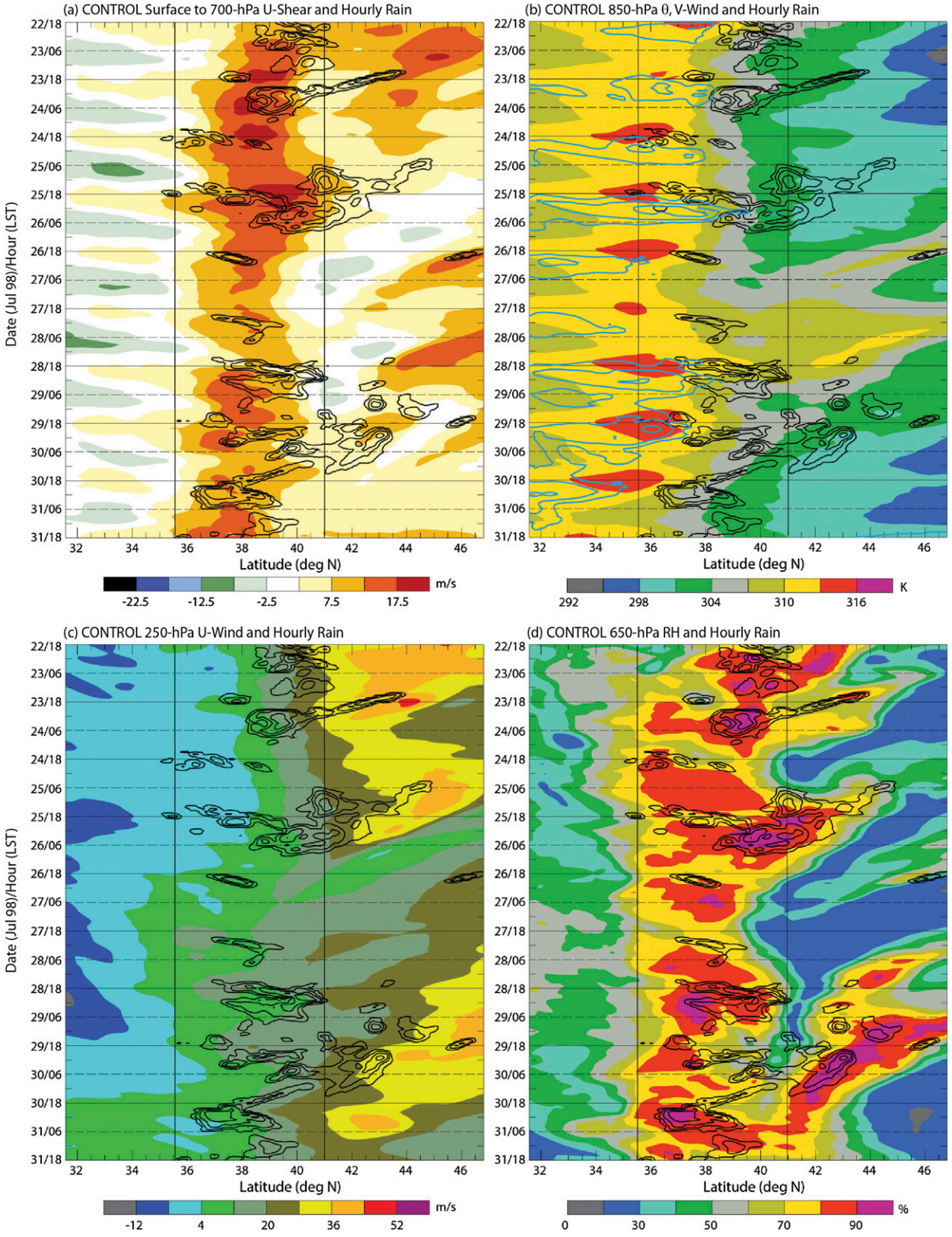

FIG. 14. As in Fig. 4, but constructed using 1-hourly outputs from CONTROL.

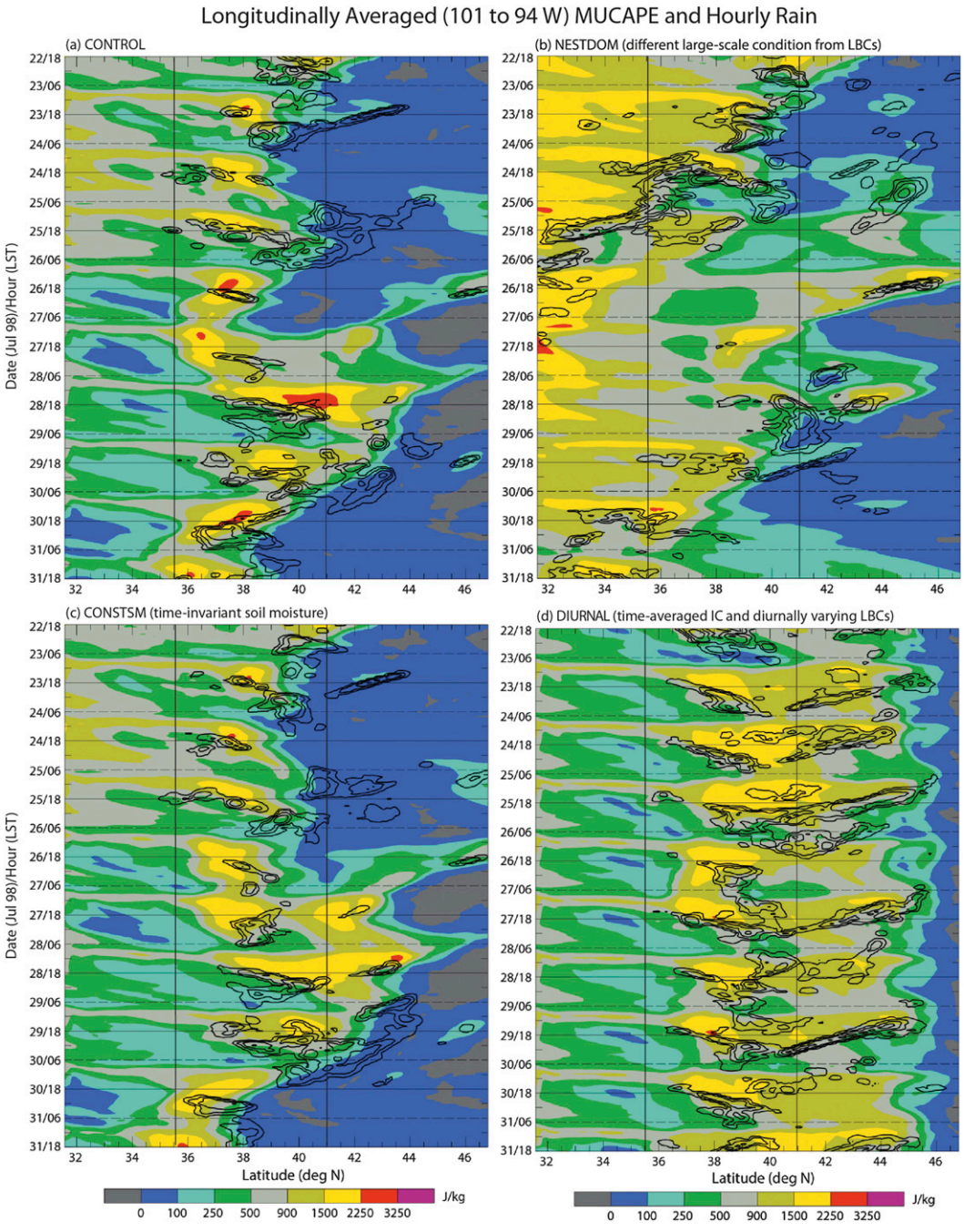

FIG. 15. Time–latitude diagrams of the most unstable (highest θ_e) CAPE for (a) CONTROL, (b) NESTDOM, (c) CONSTSM, and (d) DIURNAL, longitudinally averaged over the region indicated by the solid black vertical lines in Fig. 9. The black contours in each panel indicate where longitudinally averaged hourly rainfall exceeds 0.2, 0.6, 1.4, and 3 mm h^{-1}.

c. *Internal and external influences on corridor lower-tropospheric baroclinicity*

The results of section 5 and the previous subsection have collectively established the importance of the nocturnal LLJ interacting with a strong and quasi-stationary lower-tropospheric front as a critical forcing component for the long-lived nocturnal precipitation corridor. Figure 18 illustrates the 9-day-averaged MUCAPE and ~400 m AGL winds and θ at 0000 UTC, prior to the corridor nocturnal precipitation maximum in the high-resolution simulations (Fig. 8). Both CONTROL (Fig. 18a) and

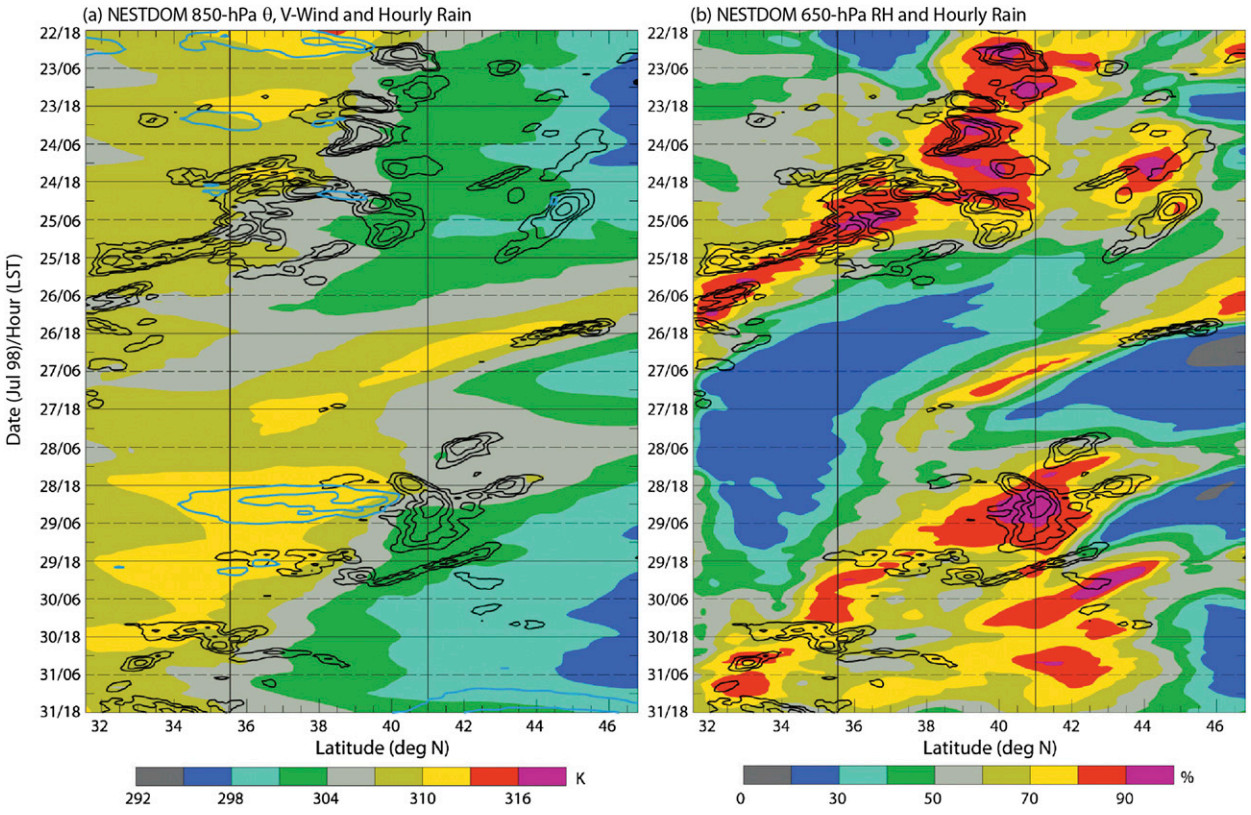

FIG. 16. Time–latitude diagrams of the (a) 850-hPa potential temperature and (b) 650-hPa relative humidity from NESTDOM longitudinally averaged over the region indicated by the solid black vertical lines in Fig. 9. The black contours in each panel indicate where longitudinally averaged hourly rainfall exceeds 0.2, 0.6, 1.4, and 3 mm h^{-1} and the cyan contours in (a) indicate longitudinally averaged 850-hPa meridional wind speeds exceeding 7.5, 10, 12.5, and 15 m s^{-1}.

CONSTSM (Fig. 18b) clearly have a much stronger time-averaged front than does NESTDOM (Fig. 18c) as well as larger values of MUCAPE in the baroclinic zone that lies immediately south of the zone of maximum nocturnal precipitation in each of the simulations. These differences among simulations may be at least partly attributed to the greater transience in NESTDOM, which arises from differences in the external large-scale forcing discussed in the previous subsection. However, we must also consider the differing degree, among simulations, of internal feedbacks that could arise from differences in the latitudinal stationarity of the precipitation corridor.

CONSTSM was designed to evaluate whether differences in the partition of surface sensible and latent heat fluxes (LE) resulting from local increases in soil moisture was a significant factor in sustaining the corridor. Comparing CONTROL to CONSTSM reveals neither the lower-tropospheric baroclinicity (Figs. 18a,b) nor the overall characteristics of the precipitation (Figs. 7b,c) are changed significantly by the 12-day soil moisture evolution in CONTROL.

In the hypothetical case of identical incoming solar radiation, the lack of soil moisture evolution in CONSTSM would result in a greater percentage, than for CONTROL, of the total surface flux ($H + LE$) to occur as sensible heat flux H, as opposed to the latent heat flux, in the northern part of the baroclinic zone where nocturnal precipitation occurs. This is confirmed by a surface heat budget (Table 3) calculated for the two rectangular regions of the simulations indicated in Fig. 18. However, the soil moisture represents only one aspect of the land–atmosphere system that can be influenced by repeated rains in the same location for such an extended period.

Here, frontogenetic latitudinal gradients in daytime H are most influenced by latitudinal gradients in downwelling shortwave radiation at the ground (SWDOWN) in CONTROL and CONSTSM, which are much larger than in NESTDOM (Table 3). These differences, which are consistent with larger latitudinal outgoing longwave radiation (OLR) gradients, result from enhanced daytime cloudiness in the wake of more frequent nocturnal corridor precipitation in the north part of the baroclinic zone in CONTROL and CONSTSM than in NESTDOM.

Though frontogenetic, the foregoing internal feedback is augmented (and perhaps exceeded) by the effect of stronger lower-tropospheric flow deformation (e.g., Fig. 18b)

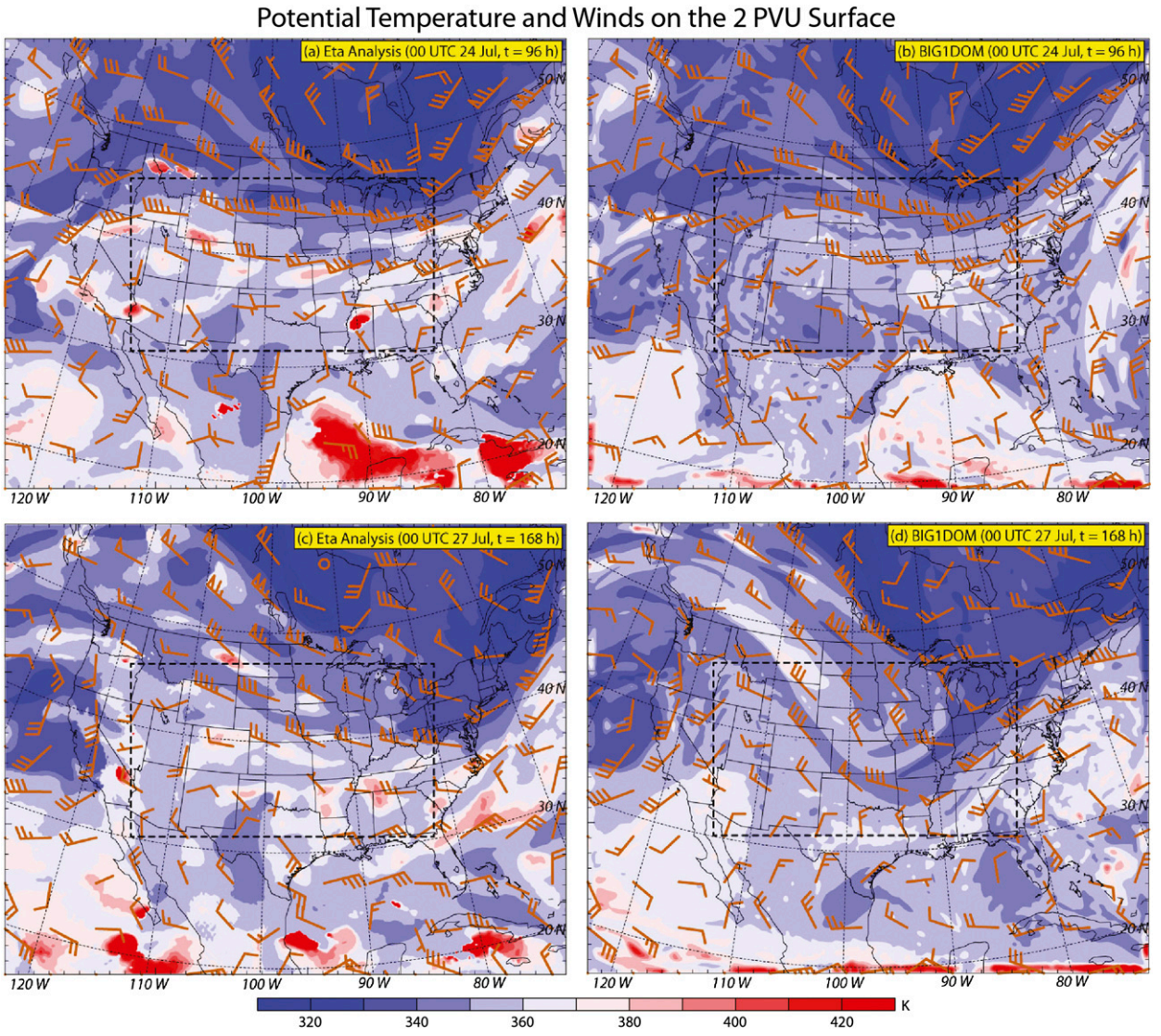

FIG. 17. Potential temperature and horizontal winds on the 2-PVU surface approximating the dynamic tropopause at (a),(b) 0000 UTC 24 Jul and (c),(d) 0000 UTC 27 Jul 1998 from (a),(c) Eta Model analyses and (b),(d) BIG1DOM. The dashed insets in each panel show the location of the high-resolution domain for the corresponding CONTROL and NESTDOM simulations.

in both CONTROL and CONSTSM. Augustine and Caracena (1994) indicated that frontogenesis is an important precursor to significant nocturnal MCS development and Trier et al. (2006) found it to influence environmental vertical motions in a previously simulated long-lived precipitation corridor.

The strong lower-tropospheric baroclinicity, deformation, and implied frontogenesis are factors common to a broader class of elevated thunderstorms occurring above shallow fronts (Colman 1990a,b). However, in both the TD06 climatology and in the current long-lived heavy precipitation corridor, anticyclonic upper-tropospheric conditions and significant CAPE contrast with typical environments of elevated convection reported by Colman (1990a,b). Such differences are not surprising considering that heavy precipitation corridors in both the current case and in TD06 occur in midsummer, during a distinct seasonal minimum in the frequency of more general elevated frontal convection, as defined by Colman (1990a, see their Fig. 4).

7. Summary and discussion

This study has utilized observations and simulations with a convection-permitting model to examine factors governing the location, persistence, and diurnal cycle of rainfall within a 12-day heavy precipitation period in the central United States. Herein, we have concentrated on

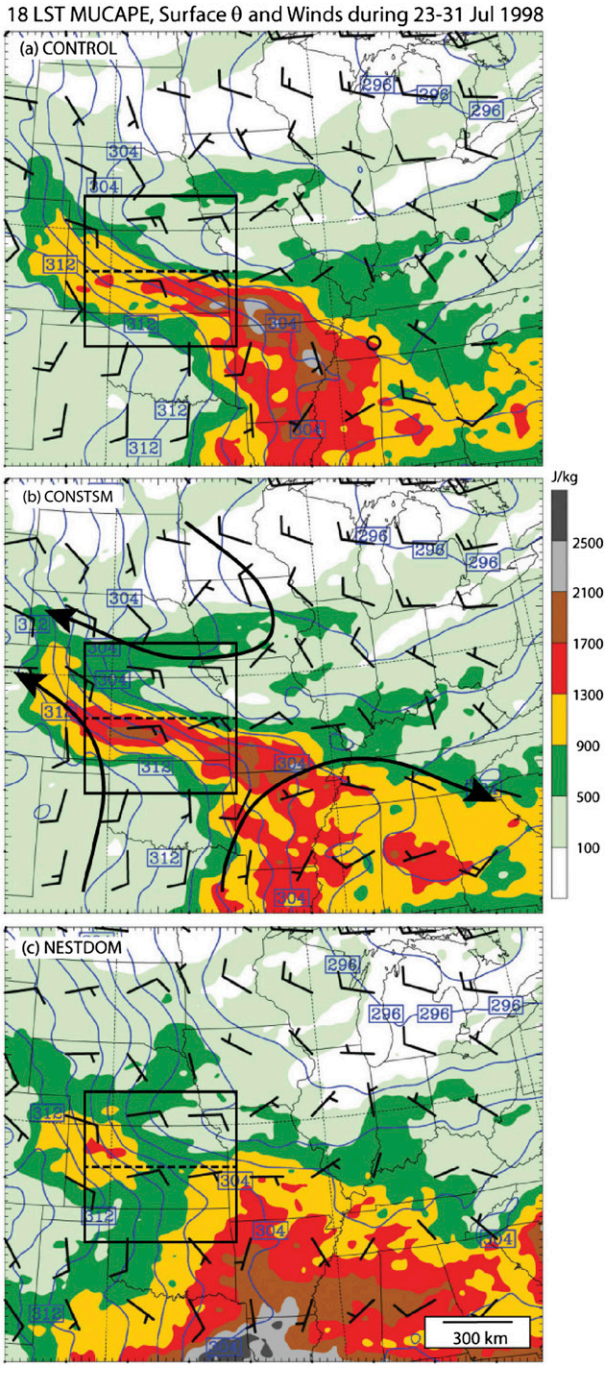

FIG. 18. 9-day-averaged 0000 UTC CAPE of the most unstable (highest θ_e) parcel, near-surface winds, and potential temperature (2-K contour interval) for (a) CONTROL, (b) CONSTSM, and (c) NESTDOM. The two rectangles separated by the dashed line in each panel denote the north and south parts of the lower-tropospheric baroclinic zone for which surface heat budgets are presented in Table 3. The arrows in (b) schematically illustrate the strong deformation referred to in the text.

a 9-day portion of this period when the rainfall location was most stationary (23–31 July 1998). Rainfall during this period was primarily nocturnal and exceeded 100 mm (with isolated regions exceeding 200 mm) in a nearly continuous band from −100° to −90° longitude. However, the latitudinal width of the rainfall band exceeding 100 mm was ~0.5°–1°, while the width of any appreciable precipitation was 3° or less. As such, this event constitutes a relatively low-frequency, yet mesoscale, phenomenon.

A strong but shallow front, an enhanced nocturnal LLJ, and a large-scale upper-level anticyclone are environmental factors in the current long-lived corridor, which also occur in the TD06 climatology of multiday warm-season precipitation corridors. Herein, we have extended the results from TD06 by 1) documenting the diurnal cycle of an observed corridor and 2) elucidating the roles of both external environmental factors and internal factors on the corridor intensity, persistence, and latitudinal confinement. Here, the external factors include both the environmental synoptic upper-tropospheric anticyclone and weak transient disturbances (e.g., midtropospheric short waves) passing through the large-scale environment, while internal factors include both patterns of residual daytime cloudiness in the wake of nocturnal convection and the evolution of soil wetness within the corridor region.

Composite analysis of the control simulation (CONTROL) revealed that hot, dry air originating in the daytime PBL required significant vertical displacements prior to being able to support convection. These vertical displacements occurred later in the diurnal cycle and within the southerly nocturnal LLJ, allowing deep convection with a narrow latitudinal corridor several hundreds of kilometers north of the leading edge of the shallow, but intense lower-tropospheric front.

The nightly precipitation within the narrow rainfall corridor resulted in large local increases in soil moisture. The CONSTSM simulation, however, revealed that soil moisture evolution during the 12-day simulation had little effect on corridor precipitation. Though daytime surface sensible heat flux gradients associated with soil moisture increases on the north side of the lower-tropospheric baroclinic zone were weakly frontogenetic in CONTROL, they were overwhelmed by those of the same sign arising from meridional gradients in downwelling shortwave radiation related to residual daytime cloudiness in the wake of the nocturnal convection.

The time-averaged differential surface heating was significant in both CONTROL and CONSTSM and reinforced the strong lower-tropospheric front, which when interacting with the nocturnal LLJ accounted for the strong vertical motions that were critical in forcing the nighttime rains. Thus, the frontogenetic effect from

TABLE 3. Daytime averages ($W m^{-2}$) from 0800 to 1800 LST over the north and south sections of the rectangles in Fig. 18 of downwelling shortwave radiation incident at the ground (SWDOWN), total surface flux ($H + LE$), surface sensible heat flux (H), surface LE, and OLR at the top of the atmosphere.

Simulation (frontal area)	SWDOWN	$H + LE$	H	LE	OLR
CONTROL					
North	437.5	276.6	107.7	168.9	253.4
South	607.4	347.4	196.3	151.1	275.2
South − north	169.9	70.8	88.6	−17.8	21.8
CONSTSM					
North	444.8	282.8	120.5	162.3	247.8
South	601.4	345.9	192.3	153.6	276.4
South − north	156.6	63.1	71.8	−8.7	28.6
NESTDOM					
North	508.4	313.5	127.0	186.5	259.6
South	600.9	345.1	189.3	155.8	272.7
South − north	92.5	31.6	62.3	−30.7	13.1

differential incoming solar radiation is considered along with midtropospheric moistening from nightly convection as one of the important factors resulting from internal feedbacks that help prolong the heavy precipitation corridor. However, an important distinction between soil moisture and insolation gradients is that the latter has no long-term memory that might persist beyond a change in the synoptic-scale flow.

External atmospheric factors appear to play an even more substantial role than do the aforementioned internal factors in the location and persistence of the corridor. Here, synoptic-scale flow deformation contributes to the strong lower-tropospheric front. Moreover, CONTROL suggests that the narrow width of the corridor is regulated by depletions of CAPE and midtropospheric moisture on its north side behind transient mid- to upper-tropospheric disturbances in the westerlies, and a more permanent absence of CAPE and midtropospheric moisture underneath the persistent large-scale upper-level anticyclone on its south side.

NESTDOM, containing a degraded lateral boundary condition, and DIURNAL, with only diurnal forcing on the boundary, constitute perturbations from CONTROL with enhanced and reduced synoptic-scale transience, respectively. With transients enhanced, meridional excursions of water vapor disrupt the corridor, and rainfall decreases over the domain. Without transients, the corridor is free to expand poleward and rainfall increases overall. Thus, the existence of a narrow corridor may depend on a delicate balance wherein *weak* transient disturbances counteract the warm-season tendency of the central United States to destabilize over time with respect to moist convection. It also may be concluded that in this regime, transient disturbances decrease the total (i.e., domain averaged) rainfall, despite the fact that they can locally increase rainfall when properly phased in the diurnal cycle.

The strong sensitivity to changes in relatively weak synoptic-scale upper-tropospheric patterns underscores the formidable challenges when making extended-range predictions of these important precipitation producers. Long-lived corridors, such as the one examined in this study, together with more common shorter-lived (1–2 day) corridors, constitute a significant fraction of the overall warm-season precipitation in affected areas. Moreover, physical processes that contribute to the localization and intensity of these corridors have an adverse effect on precipitation in surrounding areas, which heightens their regional hydrologic importance.

Acknowledgments. This research was performed as part of NCAR's Water System Program, which is supported by the National Science Foundation. The authors thank Sherrie Frederick (NCAR) for assistance in running simulations and Mukul Tewari (NCAR) for his efforts in helping to set up simulation CONSTSM. We are grateful to Russ Schumacher (Colorado State University) and two anonymous reviewers for their constructive comments that helped improve the paper.

REFERENCES

Arritt, R. W., T. D. Rink, M. Segal, D. P. Todey, C. A. Clark, M. J. Mitchell, and K. M. Labas, 1997: The Great Plains low-level jet during the warm season of 1993. *Mon. Wea. Rev.,* **125,** 2176–2192, doi:10.1175/1520-0493(1997)125<2176:TGPLLJ>2.0.CO;2.

Augustine, J. A., and F. Caracena, 1994: Lower-tropospheric precursors to nocturnal MCS development over the central United States. *Wea. Forecasting,* **9,** 116–135, doi:10.1175/1520-0434(1994)009<0116:LTPTNM>2.0.CO;2.

Brandes, E. A., 1990: Evolution and structure of the 6–7 May 1985 mesoscale convective system and associated vortex. *Mon. Wea. Rev.,* **118,** 109–127, doi:10.1175/1520-0493(1990)118<0109:EASOTM>2.0.CO;2.

Bryan, G. H., J. C. Wyngaard, and J. M. Fritsch, 2003: Resolution requirements for the simulation of deep moist convection. *Mon. Wea. Rev.,* **131,** 2394–2416, doi:10.1175/1520-0493(2003)131<2394:RRFTSO>2.0.CO;2.

Carbone, R. E., and J. D. Tuttle, 2008: Rainfall occurrence in the U.S. warm season: The diurnal cycle. *J. Climate,* **21,** 4132–4146, doi:10.1175/2008JCLI2275.1.

——, ——, D. A. Ahijevych, and S. B. Trier, 2002: Inferences of predictability associated with warm-season precipitation episodes. *J. Atmos. Sci.,* **59,** 2033–2056, doi:10.1175/1520-0469(2002)059<2033:IOPAWW>2.0.CO;2.

Chen, F., and J. Dudhia, 2001: Coupling an advanced land surface hydrology model with the Penn State–NCAR MM5 modeling system. Part I: Model implementation and sensitivity. *Mon. Wea. Rev.,* **129,** 569–585, doi:10.1175/1520-0493(2001)129<0569:CAALSH>2.0.CO;2.

——, and Coauthors, 2007: Description and evaluation of the characteristics of the NCAR high-resolution land data assimilation

system. *J. Appl. Meteor. Climatol.,* **46,** 694–713, doi:10.1175/JAM2463.1.

Colman, B. R., 1990a: Thunderstorms above frontal surfaces in environments without positive CAPE. Part I: A climatology. *Mon. Wea. Rev.,* **118,** 1103–1121, doi:10.1175/1520-0493(1990)118<1103:TAFSIE>2.0.CO;2.

——, 1990b: Thunderstorms above frontal surfaces in environments without positive CAPE. Part II: Organization and instability mechanisms. *Mon. Wea. Rev.,* **118,** 1123–1144, doi:10.1175/1520-0493(1990)118<1123:TAFSIE>2.0.CO;2.

Cotton, W. C., M.-S. Lin, R. L. McAnelly, and C. J. Tremback, 1989: A composite model of mesoscale convective complexes. *Mon. Wea. Rev.,* **117,** 765–783, doi:10.1175/1520-0493(1989)117<0765:ACMOMC>2.0.CO;2.

Davis, C. A., K. W. Manning, R. E. Carbone, S. B. Trier, and J. D. Tuttle, 2003: Coherence of warm-season continental rainfall in numerical weather prediction models. *Mon. Wea. Rev.,* **131,** 2667–2679, doi:10.1175/1520-0493(2003)131<2667:COWCRI>2.0.CO;2.

Dudhia, J., 1989: Numerical study of convection observed during the Winter Monsoon Experiment using a mesoscale two-dimensional model. *J. Atmos. Sci.,* **46,** 3077–3107, doi:10.1175/1520-0469(1989)046<3077:NSOCOD>2.0.CO;2.

Ek, M. B., K. E. Mitchell, Y. Lin, E. Rogers, P. Grummann, V. Koren, G. Gayno, and J. D. Tarpley, 2003: *J. Geophys. Res.,* **108,** 8851, doi:10.1029/2002JD003296.

Findell, K. L., and E. A. B. Eltahir, 2003a: Atmospheric controls on soil-moisture boundary layer interactions. Part I: Framework development. *J. Hydrometeor.,* **4,** 522–569, doi:10.1175/1525-7541(2003)004<0552:ACOSML>2.0.CO;2.

——, and ——, 2003b: Atmospheric controls on soil-moisture boundary layer interactions. Part II: Feedback within the continental United States. *J. Hydrometeor.,* **4,** 570–583, doi:10.1175/1525-7541(2003)004<0570:ACOSML>2.0.CO;2.

Fortune, M. A., W. R. Cotton, and R. I. McAnelly, 1992: Frontal-wave-like evolution in some mesoscale convective complexes. *Mon. Wea. Rev.,* **120,** 1279–1300, doi:10.1175/1520-0493(1992)120<1279:FWLEIS>2.0.CO;2.

Fritsch, J. M., R. J. Kane Jr., and C. R. Chelius, 1986: The contribution of mesoscale convective weather systems to the warm-season precipitation in the United States. *J. Climate Appl. Meteor.,* **25,** 1333–1345, doi:10.1175/1520-0450(1986)025<1333:TCOMCW>2.0.CO;2.

Fulton, R. A., J. P. Breidenbach, D.-J. Seo, D. A. Miller, and T. O'Bannon, 1998: The WSR-88D rainfall algorithm. *Wea. Forecasting,* **13,** 377–395, doi:10.1175/1520-0434(1998)013<0377:TWRA>2.0.CO;2.

Hong, S.-Y., J. Dudhia, and S.-H. Chen, 2004: A revised approach to ice microphysical processes for the bulk parameterization of clouds and precipitation. *Mon. Wea. Rev.,* **132,** 103–120, doi:10.1175/1520-0493(2004)132<0103:ARATIM>2.0.CO;2.

Houze, R. A., Jr., B. F. Smull, and P. Dodge, 1990: Mesoscale organization of springtime rainstorms in Oklahoma. *Mon. Wea. Rev.,* **118,** 613–654, doi:10.1175/1520-0493(1990)118<0613:MOOSRI>2.0.CO;2.

James, R. P., and P. M. Markowski, 2010: A numerical investigation of the effects of dry air aloft on deep convection. *Mon. Wea. Rev.,* **138,** 140–161, doi:10.1175/2009MWR3018.1.

Janjić, Z. I., 2002: Nonsingular implementation of the Mellor-Yamada Level 2.5 Scheme in the NCEP Meso model. NCEP Office Note 437, 61 pp. [Available online at http://www.emc.ncep.noaa.gov/officenotes/newernotes/on437.pdf.]

Kane, R. J., Jr., C. R. Chelius, and J. M. Fritsch, 1987: Precipitation characteristics of mesoscale convective weather systems. *J. Climate Appl. Meteor.,* **26,** 1345–1357, doi:10.1175/1520-0450(1987)026<1345:PCOMCW>2.0.CO;2.

Koster, R. D., and Coauthors, 2004: Regions of strong coupling between soil moisture and precipitation. *Science,* **305,** 1138–1140, doi:10.1126/science.1100217.

Maddox, R. A., 1980: Mesoscale convective complexes. *Bull. Amer. Meteor. Soc.,* **61,** 1374–1387, doi:10.1175/1520-0477(1980)061<1374:MCC>2.0.CO;2.

——, 1983: Large-scale meteorological conditions associated with midlatitude mesoscale convective complexes. *Mon. Wea. Rev.,* **111,** 1475–1493, doi:10.1175/1520-0493(1983)111<1475:LSMCAW>2.0.CO;2.

Mlawer, E. J., S. J. Taubman, P. D. Brown, M. J. Iacono, and S. A. Clough, 1997: Radiative transfer for inhomogeneous atmosphere: RRTM, a validated correlated-k model for the longwave. *J. Geophys. Res.,* **102,** 16 663–16 682, doi:10.1029/97JD00237.

NCDC, 1998: *Storm Data.* Vol. 40, No. 7, 281 pp. [Available from National Climatic Data Center, 151 Patton Ave., Asheville, NC 28801-5001.]

Rasmussen, K. L., and R. A. Houze Jr., 2011: Orogenic convection in subtropical South America as seen by the TRMM satellite. *Mon. Wea. Rev.,* **139,** 2399–2420, doi:10.1175/MWR-D-10-05006.1.

Rotunno, R., J. B. Klemp, and M. L. Weisman, 1988: A theory for strong, long-lived squall lines. *J. Atmos. Sci.,* **45,** 463–485, doi:10.1175/1520-0469(1988)045<0463:ATFSLL>2.0.CO;2.

Schumacher, R. S., and R. H. Johnson, 2005: Organization and environmental properties of extreme-rain producing mesoscale convective systems. *Mon. Wea. Rev.,* **133,** 961–976, doi:10.1175/MWR2899.1.

Scott, J. D., and S. A. Rutledge, 1995: Doppler radar observations of an asymmetric mesoscale convective system and associated vortex couplet. *Mon. Wea. Rev.,* **123,** 3437–3457, doi:10.1175/1520-0493(1995)123<3437:DROOAA>2.0.CO;2.

Skamarock, W. C., and J. B. Klemp, 2008: A time-split nonhydrostatic atmospheric model for weather research and forecasting applications. *J. Comput. Phys.,* **227,** 3465–3485, doi:10.1016/j.jcp.2007.01.037.

Smull, B. F., and J. A. Augustine, 1993: Multiscale analysis of a mature mesoscale convective complex. *Mon. Wea. Rev.,* **121,** 103–132, doi:10.1175/1520-0493(1993)121<0103:MAOAMM>2.0.CO;2.

Stensrud, D. J., 1996: The importance of low-level jets to climate: A review. *J. Climate,* **9,** 1698–1711, doi:10.1175/1520-0442(1996)009<1698:IOLLJT>2.0.CO;2.

Stumpf, G. J., R. H. Johnson, and B. F. Smull, 1991: The wake low in a mesoscale convective system having complex convective organization. *Mon. Wea. Rev.,* **119,** 134–158, doi:10.1175/1520-0493(1991)119<0134:TWUIAM>2.0.CO;2.

Sun, J., and F. Zhang, 2012: Impacts of mountain-plains solenoid on diurnal variations of rainfalls along the mei-yu front over the east China plains. *Mon. Wea. Rev.,* **140,** 379–397, doi:10.1175/MWR-D-11-00041.1.

Tao, W.-K., and Coauthors, 2013: Precipitation intensity and variation during MC3E: A numerical modeling study. *J. Geophys. Res. Atmos.,* **118,** 7199–7218, doi:10.1002/jgrd.50410.

Tiedtke, M., 1989: A comprehensive mass flux scheme for cumulus parameterization in large-scale models. *Mon. Wea. Rev.,* **117,** 1779–1800, doi:10.1175/1520-0493(1989)117<1779:ACMFSF>2.0.CO;2.

Trier, S. B., and D. B. Parsons, 1993: Evolution of environmental conditions preceding the development of a nocturnal mesoscale

convective complex. *Mon. Wea. Rev.,* **121,** 1078–1098, doi:10.1175/1520-0493(1993)121<1078:EOECPT>2.0.CO;2.

——, C. A. Davis, D. A. Ahijevych, M. L. Weisman, and G. H. Bryan, 2006: Mechanisms supporting long-lived episodes of propagating nocturnal convection within a 7-day WRF model simulation. *J. Atmos. Sci.,* **63,** 2437–2461, doi:10.1175/JAS3768.1.

——, F. Chen, K. W. Manning, M. A. LeMone, and C. A. Davis, 2008: Sensitivity of the PBL and precipitation in 12-day simulations of warm-season convection using different land surface models and soil wetness conditions. *Mon. Wea. Rev.,* **136,** 2321–2343, doi:10.1175/2007MWR2289.1.

——, C. A. Davis, and D. A. Ahijevych, 2010: Environmental controls on the simulated diurnal cycle of warm-season precipitation in the continental United States. *J. Atmos. Sci.,* **67,** 1066–1090, doi:10.1175/2009JAS3247.1.

——, ——, ——, and K. W. Manning, 2014a: Use of the parcel buoyancy minimum (B_{min}) to diagnose simulated thermodynamic destabilization. Part I: Methodology and case studies of MCS initiation environments. *Mon. Wea. Rev.,* **142,** 945–966, doi:10.1175/MWR-D-13-00272.1.

——, ——, ——, and ——, 2014b: Use of the parcel buoyancy minimum (B_{min}) to diagnose simulated thermodynamic destabilization. Part II: Composite analysis of mature MCS environments. *Mon. Wea. Rev.,* **142,** 967–990, doi:10.1175/MWR-D-13-00273.1.

Tuttle, J. D., and C. A. Davis, 2006: Corridors of warm season precipitation in the central United States. *Mon. Wea. Rev.,* **134,** 2297–2317, doi:10.1175/MWR3188.1.

——, and ——, 2013: Modulation of the diurnal cycle of warm-season precipitation by short-wave troughs. *J. Atmos. Sci.,* **70,** 1710–1726, doi:10.1175/JAS-D-12-0181.1.

Wallace, J. M., 1975: Diurnal variations in precipitation and thunderstorm frequency over the conterminous United States. *Mon. Wea. Rev.,* **103,** 406–419, doi:10.1175/1520-0493(1975)103<0406:DVIPAT>2.0.CO;2.

Wang, C.-C., G. T.-J. Chen, and R. E. Carbone, 2004: A climatology of warm-season cloud patterns over East Asia based on GMS infrared brightness temperature observations. *Mon. Wea. Rev.,* **132,** 1606–1629, doi:10.1175/1520-0493(2004)132<1606:ACOWCP>2.0.CO;2.

——, ——, H.-L. Huang, R. E. Carbone, and S.-W. Chang, 2012: Synoptic conditions associated with propagating and non-propagating cloud/rainfall episodes during the warm season over the East Asian continent. *Mon. Wea. Rev.,* **140,** 721–747, doi:10.1175/MWR-D-11-00067.1.

——, J. C.-S. Shu, G. T.-J. Chen, and D.-I. Lee, 2014: A study of two propagating heavy-rainfall episodes near Taiwan during SoWMEX/TiMREX IOP-8 in June 2008. Part I: Synoptic evolution, episode propagation, and model control simulation. *Mon. Wea. Rev.,* **142,** 2619-2643, doi:10.1175/MWR-D-13-00331.1.

Weaver, S. J., and S. Nigam, 2011: Recurrent supersynoptic evolution of the Great Plains low-level jet. *J. Climate,* **24,** 575–582, doi:10.1175/2010JCLI3445.1.

Wetzel, P. J., W. R. Cotton, and R. L. McAnelly, 1983: A long-lived mesoscale convective complex. Part II: Evolution and structure of the mature complex. *Mon. Wea. Rev.,* **111,** 1919–1937, doi:10.1175/1520-0493(1983)111<1919:ALLMCC>2.0.CO;2.

Zhang, Y., and S. A. Klein, 2010: Mechanisms affecting the transition from shallow to deep convection over land: Inferences from observations of the diurnal cycle collected at the ARM southern Great Plains site. *J. Atmos. Sci.,* **67,** 2943–2959, doi:10.1175/2010JAS3366.1.